CHALMERS
UNIVERSITY OF TECHNOLOGY

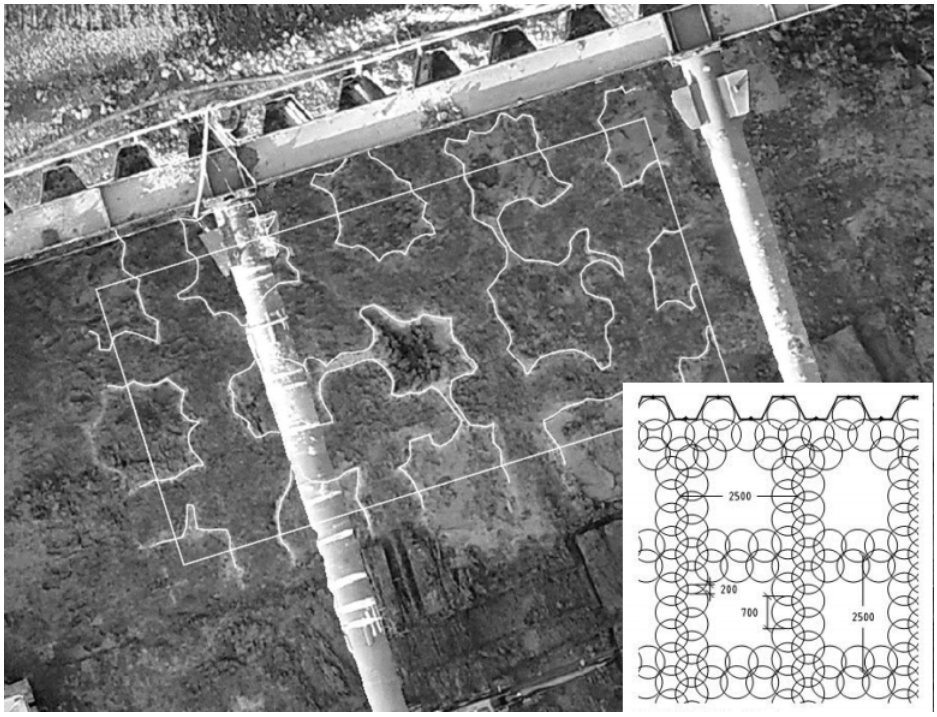

Modelling deep mixing on the passive side of a deep excavation in soft soil

A pilot study to evaluate the effect of lime-cement columns on the passive side of excavation in soft soil

S M Shazeebur Rahman

Department of Architecture and Civil Engineering
CHALMERS UNIVERSITY OF TECHNOLOGY
Master's thesis ACEX30
Gothenburg, Sweden 2020

Master's thesis ACEX30

Modelling deep mixing on the passive side of a deep excavation in soft soil

A pilot study to evaluate the effect of lime-cement columns on the passive side of excavation in soft soil

S M Shazeebur Rahman

CHALMERS
UNIVERSITY OF TECHNOLOGY

Department of Architecture and Civil Engineering
Division of Geology and Geotechnics
Chalmers University of Technology
Gothenburg, Sweden 2020

Modelling deep mixing on the passive side of a deep excavation in soft soil
A pilot study to evaluate the effect of lime-cement columns on the passive side of excavation in soft soil

S M Shazeebur Rahman

Supervisor:
Professor Minna Karstunen and
Jonatan Isaksson
Department of Architecture and Civil Engineering
Examiner:
Professor Minna Karstunen,
Department of Architecture and Civil Engineering

Department of Architecture and Civil Engineering
Division of Geology and Geotechnics
Chalmers University of Technology
SE-412 96 Gothenburg
Telephone +46 31 772 1000

Cover: Top view of the excavation at level -7 where lime-cement stabilized soil is marked [41]

Typeset in LaTeX
Department of Architecture and Civil Engineering
Gothenburg, Sweden 2020

Modelling deep mixing on the passive side of a deep excavation in soft soil
A pilot study to evaluate the effect of lime-cement columns on the passive side of excavation in soft soil

S M SHAZEEBUR RAHMAN
Department of Architecture and Civil Engineering
Division of Geology and Geotechnics
Chalmers University of Technology

Abstract

Lime-cement (LC) columns was recently adapted to stabilize the passive side of a excavation in soft soil in Sweden within the railway project Västlänken. Inclinometers were installed on the construction site to measure the wall displacements as well as sensors to measure the forces in the struts. To further deepen the understanding of the behavior of a LC stabilized excavation a numerical model is created using Creep-SCLAY1S model and Hardening Soil model to represent the clay and the lime-cement composite respectively. The numerical model prediction and the monitored performance of the excavation are compared and analyzed. Different stiffness parameters of the lime-cement soil block are considered to investigate the effect of stiffness changes on the model. With the adjusted stiffness parameters, the maximum outward wall displacement is approximately 40 mm after the stage LC installation and the highest inward movement is around 30 mm after dismantling the bottom strut compared to the field measurement of around 45 mm and 35 mm for the respective stages. The largest estimated forces in the top and bottom struts are 2400 kN and 2800 kN respectively where as the observed forces are approximately 2250 kN and 1700 kN. The Hardening Soil model represents the LC stabilized material in a sufficient way as the wall displacements and strut forces during the excavation is well estimated by the created model. The displacements of the retaining wall are not sensitive to LC columns stiffness during the initial construction stages but are increasingly sensitive as the excavation proceeds below level -7. The maximum bottom heave and top clay layer displacements estimated by the model are 170 mm and 115 mm upward respectively. Overall, numerical models can be a design tool for LC stabilization in the passive side of excavation in soft soil.

Keywords: västlänken project, deep excavation, soft soil, lime-cement column, CREEP-SCLAY1S, Hardening Soil model.

Acknowledgements

This Master's thesis studies the topic of deep mixing effect on the passive side of deep excavations in soft soils such as Gothenburg clay. It is based on a real case study of the deep excavation for the tunnel in Västlänken project in Gothenburg, Sweden.

I would like to thank my supervisor, **Professor Minna Karstunen** and **Jonatan Isaksson** from Chalmers University of Technology, Division of Geology and Geotechnics. It is an honor to have Minna as my supervisor as she is a pioneer in finite element modelling of soft structured clays. Jonatan helped me throughout the process from collecting the data to writing the thesis. I feel particularly grateful for his time and feedback.

I would also like to mention NCC and Trafikverket for providing the field data of Västlänken E02 project. It was nice to visit the construction site and experience the disciplined construction sequences.

It is important to recognize here my family and friends without whose lifetime support this work would not have been possible. It was difficult to migrate at Sweden for study leaving everything close to heart. But these people motivated me with their pure heart and kept me in line during these two years of study abroad.

Special acknowledgment to the department of Architecture and Civil Engineering, Chalmers University of Technology for providing me the opportunity of studying here with the **Avencez scholarship**.

S M Shazeebur Rahman,
Gothenburg, October 2020

Contents

List of Figures

List of Tables

1

Introduction

This chapter presents detailed description of the background, scopes and objectives of this current study.

1.1 Introduction

Earth carries each and every physical structure from buildings to bridges. Soil mechanics developed as human civilization move forward. In the seventeenth century, geotechnical engineering received a theoretical base with the introduction of Mohr-coloumbs theory. Modern days geotechnical mechanics began in 1925 when Karl Terzaghi the father of soil mechanics and geotechnical engineering published his research on settlements and failure in soils. With higher strength and stiffness the soil can carry higher loads and hence suitable for construction works on it. Various type of soils has been found globally and it defines the structural category of those regions. Soil varies in particle size distribution, soil mineralogy, water content, etc. Natural soil deposit consists of soil particles, water, and air. Usually, water and air fill the voids between the soil particles. In general term soils with fewer voids possess higher strength and stiffness and are hence more suitable for supporting structures. But with the increasing demand for structures and shortage of proper soil, it is necessary to build structures on soft soils.

Building structures on soft soils like silt and clay are complex as these soils are prone to differential settlement, swelling and shrinkage, liquefaction, etc. Improving the existing soft soil is an option to solve the engineering difficulties. As the necessity of infrastructures increases with time, it is desirable to improve the stiffness and load carrying capacity and to reduce settlement and lateral movements of soft structured soils. Soft soil can be improved by various methods like vibrofication, dynamic compaction, stone columns, compaction piles, grouting, vertical drainage techniques, chemical stabilization, lime-cement stabilization, fly-Ash stabilization, heating and freezing of soil, etc.

Deep mixed columns using Lime-cement is a popular technique first developed in Japan and Scandinavian countries in 1970s and later gaining more popularity around the world. The method essentially involves mixing binder (e.g. cement, lime, or other additives) with soil by some means (e.g. rotary mixing tools, or jet grouting), causing it to become hardened with a 10 to 50 fold increase in the shear strength of the original soil. The modified ground can thus be considered as a composite system of stiff stabilized soil columns and soft original soil that interacts to mobilize a combined resistance against shearing. Various patterns of columns can be installed in

the ground depending on the purpose of ground modification, the soil stratigraphy, and the performance criteria of the super-structure. The column patterns can be grouped as block type, grid type, wall type, and group column type.
Soft-structured clays are found in many regions of Sweden. The soil layers nearby to the rivers are developed from the glacial and post-glacial sedimentation which creates soft soil profiles of various properties. Gothenburg is the second-big city in Sweden and has the largest port in all Scandinavia. Almost half a million people live here and its the fastest growing regions in Northern Europe. With the aims to develop the infrastructure of the western part, to reduce the commute time in between various regions, and to increase more train routes and frequency, the Swedish Transport Administration has induced a project that consists a tunnel beside the river Göta. The västlänken project will connect commuter railroads that pass through the Gothenburg city with three new underground stations(Gothenburg Central Station, Haga, and Korsvägen). Engineering works like foundation, tunnel, bridges embankments on these soil layer need above mentioned special treatments. A special soil stabilization technique is applied with lime cement column on the passive side of the excavation for the tunnel. In this paper, the consequences of using deep mixed LC columns in the excavation will be discussed.
Designing deep excavation is a complex problem as various factors need to be considered. Soft soil is one of the factors that brings difficulties to design of excavations. Also because of the rapid urbanization, the surrounding structures need to be considered in the design process. To ensure the safety of the surrounding infrastructure and as well as the construction workers in an excavation, various techniques in design is adopted. Deep mixing columns in the passive side are one of the possible techniques to reduce excavation-induced ground movements. The first use of deep mixing in excavation work in the European region was in 1987 at Nürnberg and since 1994 it was used commercially for the construction of temporary and permanent panels supporting excavations, cut-off walls, ground improvement, and environmental purposes, etc.[22] Although deep mixing is a popular method of stabilizing soft soils, there is no well-established rules or design criteria in Sweden for the use of LC columns in the passive side of an excavation.
Numerical models are an effective tool to understand the behavior of LC columns in soft soil. With accurate numerical formulation of soil parameters, stiffness parameters of structures and stabilized soil it is possible to generate models that can predict the long and short-term deflections, settlements factor of safety, horizontal movements, change in stress conditions in various stages of geotechnical construction. Derivation of the model parameters requires knowledge of theoretical and practical geotechnical engineering. Creating numerical models using PLAXIS 2D software is a common practice in the present days. Various soil models are introduced in the program to simulate various geotechnical complexities for instance the elastic behaviors, anisotropy, hardening, creep, etc.
In this report, a Finite element model will be generated using the PLAXIS 2D program with CREEP-SCLAY1S and Hardening soil models. The required soil parameters will be derived from different field and laboratory tests for example oedometer test, triaxial compression and extention test, etc.

1.1.1 Aims

- Create an FE model in PLAXIS 2D representing the field scenario of an instrumented deep excavation in soft soil using lime-cement columns in the passive side.
- Adjust the model parameters for the LC stabilized soil block for a best fit between numerical simulation and measured performance of the structure.

1.1.2 Objectives

- Derive model parameters to represent the behavior of the clay (CREEP-SCLAY1S) and lime-cement stabilized soil (Hardening Soil).
- Study the effect of construction stages on deformations.
- Assess measured and simulated behavior of the excavation and make appropriate changes to the stiffness parameters of the LC -stabilized block.

1.1.3 Limitations

- Temperature effect on the FE model. Temperature is a factor that affects material response and it is not constant throughout the construction period. But this parameter are not considered in this modelling.
- One section of the whole excavation is considered. The width of the excavation changes at various sections and the spacing of the struts are not uniform throughout the construction. This specific section is considered as the inclinometers are installed in this unit.
- Simplification of the composite clay and LC stabilized block in 2D.

2
Background

This chapter consists of the background study of all the topics related to the thesis.

2.1 Classifications of soil

Soils with similar engineering properties can be grouped or sub-grouped together to express their characteristics in general. According to textural classification, soil is mainly of three types, sand, silt, and clay. This classification is based on the particle size which is very simple and does not consider the engineering behaviors like plasticity. Soils engineers are using more detailed classification systems that consider the particle-size distribution, atterberg limits, etc to classify the soil. Massachusetts Institute of Technology(MIT), U.S. Department of Agriculture(USDA), American Association of State Highway and Transportation Officials (AASHTO) and the Unified Soil Classification System(USCS) is the universally accepted classification systems. [4]

Table 2.1: Particle size classifications [4]

	Grain Size(mm)			
Name of Organization	Gravel	Sand	Silt	Clay
MIT	>2	2-0.06	0.06-0.002	<0.002
USDA	>2	2-0.05	0.05-0.002	<0.002
AASHTO	76.2-2	2-0.075	0.075- 0.002	<0.002
USCS	76.2-4.75	4.75-0.075	Fines(<0.075)	

These classification systems are described in detail in Principles of Geotechnical Engineering by B M Das.[4] Table 2.1 and Figure 2.1 show the ranges of particle size for various soils in the different classification systems. Soils with smaller particle sizes are usually known as soft soil. EAB(Empfehlungen des Arbeitskreis "Baugruben") of the German Geotechnical society provides some specific requirements of soft soil. Soil can be classified as soft soil if all or some of the requirements below are fulfilled. [6]

- Consistency index $I_c < 0.75$ (very soft to soft).
- Undrained shear strength $S_u \leq 40$ kN/m^2.
- Saturation (Full or partially full)
- Plasticity (High to medium)
- Thixotropic

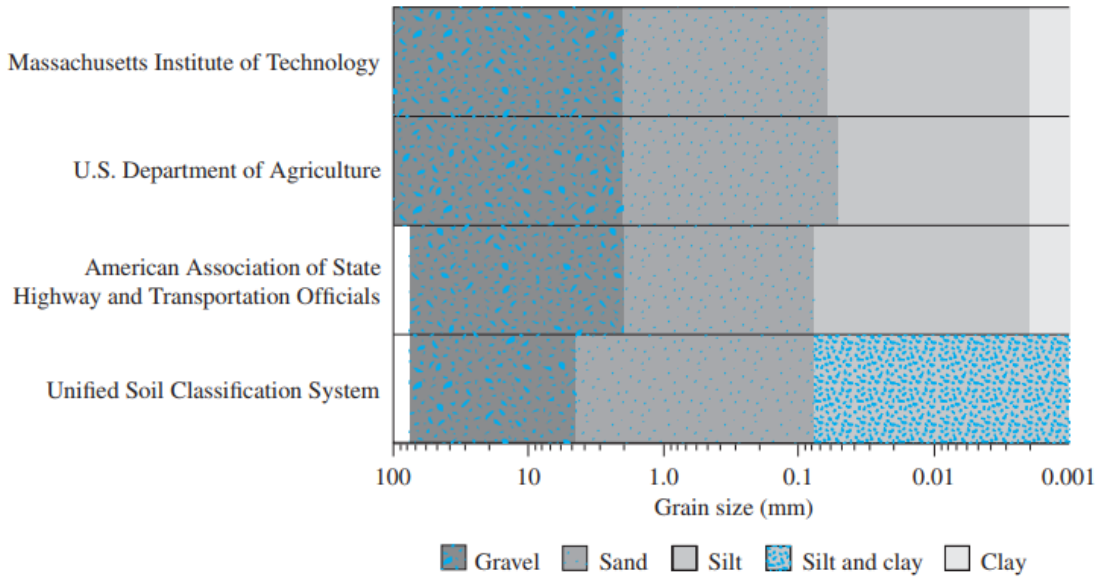

Figure 2.1: Particle size limits by various systems [4]

2.2 Excavations in soft soils

With the increasing demand for underground space, large scale excavation is a common construction practice in the modern world. Excavation deeper than 6 m is known as deep excavation according to some research. ([35] [27] [13]) Deep excavation requires sheet piles, struts, etc to support the system. Sheet piles support the active soil laterally and reduce horizontal movements of the system. Struts are often required to keep the equilibrium of retaining walls. It supports the retaining walls from overturning and reduces the chance of collapse. The structural elements carry the loads from the active soil pressure and the weights of the machinery used in the excavation. A schematic view of a deep excavation is provided in figure 2.2.

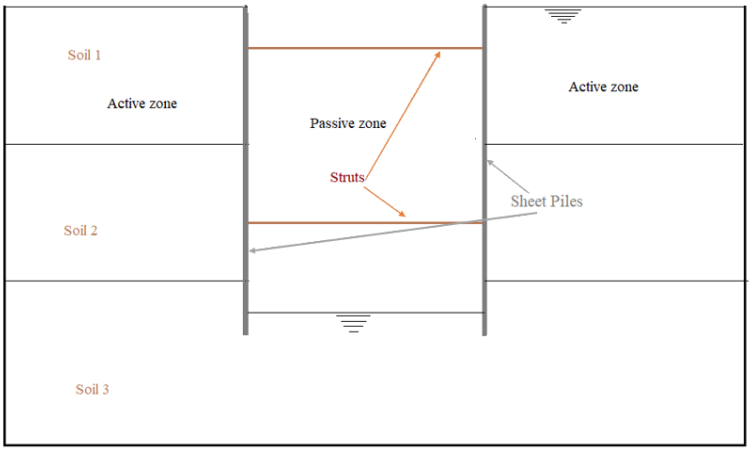

Figure 2.2: An schematic diagram of Deep excavation

From the literature it is found that the performance of deep excavation depends on

soil property, initial soil stresses, construction method and sequences, groundwater conditions, geometry and support system, etc. Two design criteria are adopted for deep excavations: (1) to stabilize the excavation using the support system; and (2) to control the ground settlement around an excavation area. The movement associated with deep excavations is related to the support system, the excavation process, and the soil properties. In case of unloading problems previous stress history of the soil is important to judge the soil response properly [18]. Effective stress changes as the pore water pressure dissipates with time. Permeability is low in clay which leads to the often used design assumption of undrained soil behaviour. This can underestimate the stability of the whole system in the long term.
Excavation in soft soil also causes bottom heave. Heave is an upward soil displacement related to the unloaded soil mass and the surrounding surcharge (Figure 2.3). Because of excavation, the total stress reduces and the expansion from unloading

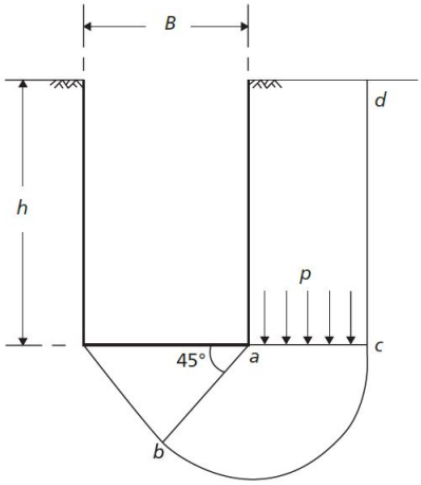

Figure 2.3: Bottom heave failure mechanism by Terzaghi [16]

causes a negative excess pore water pressure below the bottom of the excavation[16]. Previous studies provide guidelines for excavation designs considering various parameters like soil properties, stress conditions, support system, pore water pressure etc. Peck[26] developed relations(Figure 2.4) of ground settlements, u_v normalized by the depth of excavation, H against distance from the excavation for strutted and tied-back soldier walls, and sheet pile walls. Three zones were defined in the paper in terms of soil properties. Zone 1 is considered for sand and soft to hard clay, zone 2 covers very soft to hard clay at limited depth beneath excavation bottom and zone 3 defines very soft to soft clay to a significant depth bellow excavation bottom.

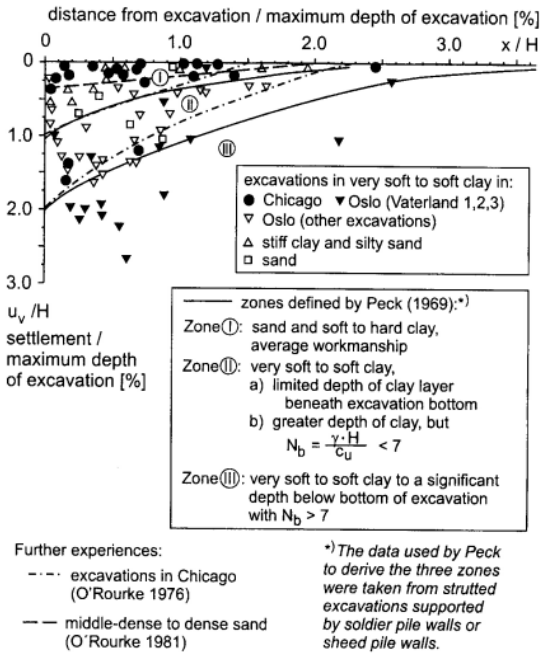

Figure 2.4: Summary of measured settlements adjacent to deep strutted excavations [26]

Later Goldberg et al.[9] analyzed 63 excavation case histories and concluded that the maximum vertical settlement behind excavations is 0.5 to 1.5 times higher than the maximum horizontal displacement of the sidewalls and in soft clay this ratio goes above 2.0 (Figure 2.5).

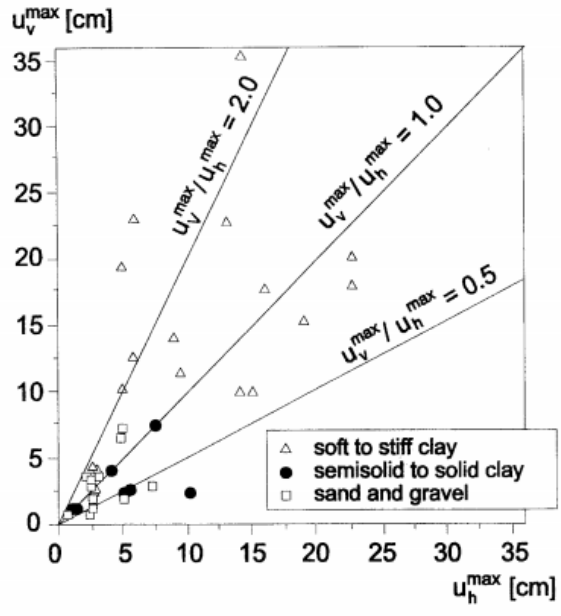

Figure 2.5: Maximum vertical settlement vs Maximum horizontal wall displacement [9]

Clough et al.[2] studied excavations in soft clays and found out that, lateral movement of retaining walls depend significantly on the factor of safety against base heave FOS_{base} and system stiffness. Researchers have been working on excavation problems continuously and found out several correlations on ground movement with soil type, structural stiffness, depth of excavation.
In 2004 Moormann [23] did an empirical case study on 530 deep excavations in soft clays (C_u< 75 kN/m^2)and concluded several points. The maximum wall movement lies between 0.5% and 1.0% of the excavation depth(H) and it is measured at a depth z= 0.5H to 1.0H below the ground surface. The maximum vertical settlement ranges from 0.1%H to 10%H and normally occurs at a distance of less then 0.5H behind the support structure. Also, settlements are dependent on the system stiffness up to a certain excavation depth. Soil type and excavation depth are identified as the most significant parameters while designing a deep excavation.
Various techniques have been considered to reduce the settlement, horizontal movement, and base heave associated with an excavation. Among those are raft foundation at the bottom, submerged excavation, and lime-cement columns are examples of utilized procedures. Improving the soil properties by deep mixing columns in the passive side of excavation reduces settlements and lateral movements and can also reduce structural forces and improve the factor of safety against basal heave failure. [12] Three approaches are considered to predict the ground movement caused by deep excavation that is empirical methods([26], [2], [42]), numerical methods([21], [11], [25]) and the analytical solutions([29], [8]). All these methods are useful in specific projects. However, numerical analysis is common to analyze the nonlinear behavior of soil and to overcome design problems in a deep excavation.

2.3 Use of lime-cement columns

Deep mixing is globally used to increase the permeability, strength and reduce deformations of soft soil. Deep mixing is a generic term for a large number of methods in which binding agents, often lime or/and cement, are mechanically mixed with the soil([19], [28], [34]). Since the late 80s, the most common binder to stabilize soil is a mixture of lime and cement, this method is known as “lime–cement columns” or “Scandinavian dry deep mixing” [33]. Two different installation methods for lime cement columns are the dry-mixing method and the modified dry-mixing method. The major difference between the methods is that binder is added as a dry powder in the dry method and it reacts with water in the soil. Soil with higher water content is suitable for this method. In the wet method, a slurry binder with water is used. The dry mixing method is commonly applied in Sweden.
The installation process involves mixing by rotating mechanical mixing tools forming circular columns of hardening soil. The columns are normally installed individually or in grids (Figure 2.6). Lime-cement columns have higher shear strength and compression modulus compared to unstabilized soil and thus improve the bearing capacity of the soil as well as reduce the consolidation settlements beneath a loaded surface.

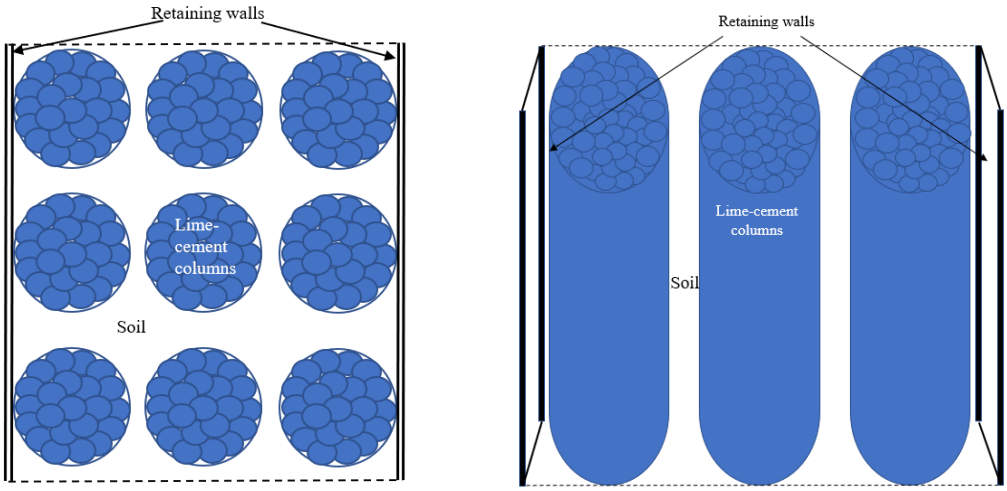

(a) Plan **(b)** Elevation

Figure 2.6: Schematic orientation of lime-cement columns installation

A case study done by R. Ignat et al.[12] shows that LC columns acted as a support for the sheet pile wall under the excavation and creates a 'strut like effect'. This paper also analyzed the failure mechanism of two LC panels with different center to center distance and concluded that higher spacing among the columns leads to brittle failure in the clay. Also, the interaction between the LC columns and soils increases with overlapping columns.

2.4 Numerical soil modeling

Numerical methods of analysis fractionated into Finite Difference Method (FDM), Finite Element Method (FEM), Boundary Element Method (BEM), Discrete Element Method (DEM), Discontinuous Layout Optimisation (DLO), Material Point Method (MPM). The methodology of these methods is different and all has its own merits and demerits. The Finite Element Method (FEM) is popular and well approved in geotechnical society.
Finite element models are being used by the geotechnical engineers to anticipate the possible soil response under any stress path. An FE model requires parameters related to soil mechanics, the geometry of the system, construction steps, boundary conditions, and stiffness of any structural members. The soil parameters are evaluated from laboratory test and field test data. Geometry and boundary conditions are simplified to reflect the problem as per the requirement of the model output that still represent the field conditions. Numerical analysis is sensitive to the choice of parameters and a correct idealization will lead the model to the possibility of representing the real soil behavior.
Several FE studies have been done on excavations in deep mixed improved soil. Improving the design mechanism and FE model of stabilized soil is necessary because the current design methods are simple and have limitations. The design methods and FE models should consider soil-structure interaction and installation effect to

predict the realistic behavior of the stabilized soil.
A few case studies have been found on FE analysis of deep excavation in Deep mixing column type ground improvement. Most of the models are created as plane strain models and the improved soft soil is considered as a composite material [24]. Yang et al.[40] describes the influence of material properties and installation grid on the degree of mobilization of the deep mixed columns. This study also illustrates the effect on the overall behavior of the structure and the type of failure mechanism because of the interaction between the LC columns and the soft soil in between the column rows.
Two soil models are considered in this present study. Creep-SCLAY1S and Hardening soil models will present the clay soil and the LC columns respectively. The detail description of these two soil models are provided below.

2.4.1 Creep-SCLAY1S model

Description

Natural soft clay shows elastic and plastic anisotropy, structure and rate- dependency, nonlinear elasticity, etc. Most of the soil models cannot portrait the anisotropy of natural soft clay which leads to inaccurate projections of soil reaction under loading. Soil anisotropy has been included in constitutive models assuming that the variation of yield curve inclination is generated by plastic volumetric strains only([1], [3], [5], [38]). These models ignored the effect of plastic shear strains which is not the real case scenario. Then wheeler et al. [37] proposed the S-CLAY1 model which is an extension of critical state models with anisotropy during plastic straining. This model is designed for normally consolidated or lightly overconsolidated soft clays which are plastic deformations dominated problems. Elastic volumetric and deviatoric strains are assumed to be isotropic in this model as in MCC. This assumption makes the model incompatible for analyzing problems where soil particles follow unloading stress paths(like excavation) and also cyclic loading. The S-CLAY1 model includes two hardening laws, firstly change of yield curve size is related only to plastic volumetric strain as in MCC and secondly, it narrates the change of yield curve inclination produced by plastic volumetric and shear straining which represents the erasure of anisotropy with plastic strains. In consequence of this inclusion, the model predicts a unique inclination of the yield curve at critical state which is realistic. Later bonding and destructuration of soil particles were added in the model and an extended version S-CLAY1S ([17], [15]) was formed. This model added new dimensions from computational point of view but creates non-convergence problems in FE analysis. Based on the S-CLAY1 model an anisotropic rate-dependent model named anisotropic creep model(ACM) was proposed by leoni[20] which accounts for the initial anisotropy and the evaluation of anisotropy.
Creep-SCLAY1S[32] model is a creep model similar to elastoplastic S-CLAY1S model. The model is presented in triaxial stress space to model the response of cross-anisotropic samples subjected to oedometric and triaxial loading paths. For the above simplification, mean effective stress, p ' and deviator stress, q are respectively defined by p '= $(\sigma'_a + 2\sigma'_r)/3$ and q= $(\sigma'_a - \sigma'_r)$. Also, the volumetric

strain rate $\dot{\varepsilon_v}$=($\dot{\varepsilon_a} + 2\dot{\varepsilon_r}$) and deviatoric strain rate $\dot{\varepsilon_q} = 2/3(\dot{\varepsilon_a} - \dot{\varepsilon_r})$ are used where subscript a and r stand for axial and radial directions. Elastic and creep strains are combined with an additive law and the total strain rate is expressed analogously to the classical elasto-plastic theory.

$$\begin{aligned} \dot{\varepsilon_v} &= (\dot{\varepsilon_v^e} + \dot{\varepsilon_v^c}) \\ \dot{\varepsilon_q} &= (\dot{\varepsilon_q^e} + \dot{\varepsilon_q^c}) \end{aligned} \tag{2.1}$$

Where, $\dot{\varepsilon}$ implies strain rate. Superscript e and c stand for elastic and creep components and subscript v and q denote volumetric and deviatoric components respectively. Elastic volumetric and deviatoric strain rate is defined by $\dot{\varepsilon_v^e}$= $\dot{p}$ '/K and $\dot{\varepsilon_q}$ = $\dot{q}$/3G respectively. Here elastic bulk modulus K= p '/κ^* and shear modulus G= 3K(1-2υ')/2(1+υ') are stress-dependent. υ' is Poisson's ratio. In this model creep deformation will always occur due to the nature of particles as it is assumed that there is no pure elastic state. Creep strain rates are defined as

$$\begin{aligned} \dot{\varepsilon_v^c} &= \dot{\Lambda}\frac{\delta p'_{\ eq}}{\delta p'} \\ \dot{\varepsilon_q^c} &= \dot{\Lambda}\frac{\delta p'_{\ eq}}{\delta q} \end{aligned} \tag{2.2}$$

$\dot{\Lambda}$ is the visco-plastic multiplier defined by

$$\dot{\Lambda} = \frac{\mu_i^*}{\tau}\left(\frac{p'_{eq}}{p'_m}\right)^{\beta}\left(\frac{M_c^2 - \alpha^2_{K_o^{nc}}}{M_c^2 - \eta^2_{K_o^{nc}}}\right) \tag{2.3}$$

where, μ_i^* is the modified intrinsic creep index and derived from the ε_v-ln t curve at high stress to confirm zero particle bonding condition. β is defined by

$$\beta = \frac{\lambda_i^* - \kappa^*}{\mu_i^*} \tag{2.4}$$

λ_i^* is the modified intrinsic compression index.
To describe the state of the soil particles, three different surfaces (Normal Consolidation Surface(NCS), Current Stress Surface(CSS), Intrinsic Compression Surface(ICS)) are used (Figure 2.7). NCS defines the boundary between small and large creep strains and CSS shows the present condition of effective stresses. The interaction between the vertical tangent to NCS and CSS with the horizontal p' axes is respectively the isotropic preconsolidation pressure p'_m and the equivalent mean stress p'_{eq} . The third boundary ICS defines the bonding effect as per Gens and Nova [7] and an has identical contour but a smaller magnitude than NCS. Current bonding among the soil particles χ is related to this shrinkage of ICS by the equation.

$$p'_m \ = p'_{mi}\,(1 + \chi) \tag{2.5}$$

where p'_{mi} is the isotropic preconsolidation pressure that defines the size of ICS.

A general equation [32] that defines all the three surfaces is,

$$p'_{size} \ = p' \ + \frac{(q - \alpha p'\,)^2}{(M^2(\theta_\alpha) - \alpha^2)p'} \tag{2.6}$$

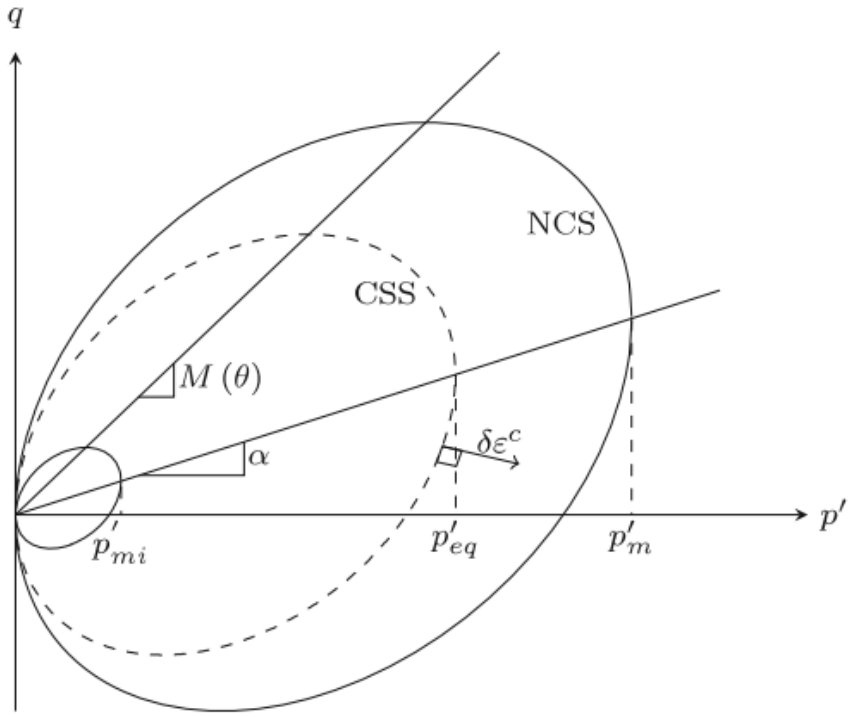

Figure 2.7: Current Stress Surface(CSS) and Normal Consolidation Surface(NCS) of the Creep-SCLAY1S soil model [10]

where p'_{size} defines the ICS, the CSS, and the NCS respectively with the change in scalar quantity α. M(θ_α) is the critical stress ratio in triaxial extension(M_e) and triaxial compression(M_c) that depends on Lode angle θ. The Lode angle formulation controls the critical state stress ration in extension and compression.[32]. Equation[31] used to define M(θ_α) is,

$$M(\theta_\alpha) = M_c \left[\frac{2m^4}{1 + m^4 + (1 - m^4)\sin 3\theta_\alpha} \right]^{\frac{1}{4}} \tag{2.7}$$

where m = M_e/M_C and should be higher than 0.6 to ensure a convex failure surface. m=1.0 refers to the Drucker-Prager failure criterion.
The Creep-SCLAY1S model considers three hardening rules that are Isotropic, structural, and rotational hardening. The first two influences the size of NCS and ICS according to the following isotropic and structural hardening rules. Isotropic hardening describes the change in intrinsic isotropic preconsolidation pressure with volumetric creep strains and structural hardening relates the debonding rate, $\dot{\chi}$ with respect to the deviatoric and volumetric creep strains rate as below.

$$\begin{aligned} \dot{p}'_{mi} &= \frac{p'_{mi}}{\lambda^*_i - \kappa^*} \dot{\varepsilon}^c_v \\ \dot{\chi} &= -a\chi \left(|\dot{\varepsilon}^c_v| + b|\dot{\varepsilon}^c_q| \right) \end{aligned} \tag{2.8}$$

Where "a" and "b" are the absolute ad relative rate of destructuration that control the bond degradation rate between soil particles because of creep strain rate. Chemical

bonding is ignored in this model.
The rotational hardening describes the change in contour of the three surfaces with creep strains with the evaluation α. The equation below describes the evaluation of anisotropy with irrecoverable strains.

$$\dot{\alpha} = \omega \left[\left(\frac{3q}{4p'} - \alpha \right) < \dot{\varepsilon_v^c} > + \omega_d \left(\frac{q}{3p'} - \alpha \right) |\dot{\varepsilon}_q^c| \right] \tag{2.9}$$

Where ω and ω_d are the absolute and relative effectiveness of rotational hardening respectively. These two parameters describe the rate of rotation of soil particles and change in fabric anisotropy caused by creep strain rate.
The initial size of CSS is calculated from the in-situ axial effective stress σ'_{oa} with in situ K_o(Lateral earth pressure at rest) and α_0(Initial inclination). In situ vertical effective stress σ'_{oa} , K_0^{nc}(Lateral earth pressure at rest for normally consolidated state), α_0, Pre-overburden pressure(POP=σ_{po}-σ'_{oa}) or over-consolidation ratio (OCR=σ_{po}/σ'_{oa}) is used to derive the initial size of the NC surface.

Parameters
Creep-SCLAY1S model requires 14 parameters, among these 11 soil constants and 3 initial state variables. The soil constants can split into conventional, anisotropic, creep, and destructuration parameters.

Initial state parameters
The initial void ratio is necessary for consolidation analysis even though it is not a model input parameter. The apparent vertical preconsolidation pressure, σ_{po} is required to calculate the POP or OCR along with in-situ vertical effective stress, σ'_{oa} . Estimating the correct σ_{po} is important as it differentiates between the elastic and inelastic deformations phase. It is advised not to use a constant rate of strain tests while calculating this value as higher strain rates will lead to an unrealistic higher preconsolidation pressure.
Lateral earth pressure at rest for NC state(K_0^{nc}) and OC state(K_0) can be calculated using various empirical formulas. The following two equations using the critical friction angle, ϕ'_{cv} is suggested by Karstunen et al. [15],

$$\begin{aligned} K_0^{nc} &= 1 - \sin\phi'_{cv}\ [Jaky's formula] \\ K_0 &= (1 - \sin\phi'_{cv}\ ) * OCR^{\sin\phi'_{cv}} \end{aligned} \tag{2.10}$$

Conventional parameters
Most of the conventional parameters are similar to the Modified Cam-Clay(MCC) model parameters (Poisson's ratio, ν' Critical stress ratio, M; Modified compression index, λ^*; Modified swelling index, κ^*)with the addition of intrinsic compression index, λ_i^*. λ^*, κ^*, λ_i^* are derived from the stress-strain curve as shown in figure 2.8. λ_i^* usually calculated from remolded clays, if remolded clay is not found then higher strain section oedometer test data can be utilized.

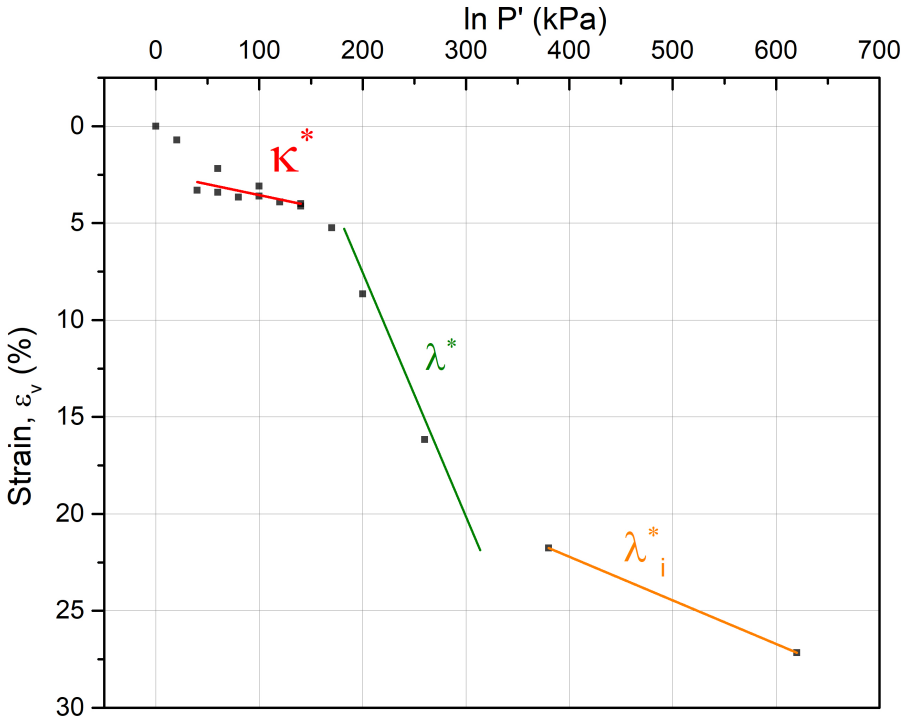

Figure 2.8: Extraction of soil parameters (λ^*, κ^*, λ_i^*) from stress-strain curve.[From Oedometer Test data of Västlänken E02 project at 15m (Borehole no. 1-03)]

M_c and M_e can be calculated using the following equations,

$$\begin{aligned} M_c &= \frac{6\sin\phi'_{cv}}{3-\sin\phi'_{cv}} \\ M_e &= \frac{6\sin\phi'_{cv}}{3+\sin\phi'_{cv}} \end{aligned} \tag{2.11}$$

In case of no triaxial extension test data, M_e can be calculated assuming friction angle in compression to be the same as in extension (Mohr-Coulomb failure criteria)[14] using the equation below.

$$\sin\phi'_c = \frac{3M_e}{6-M_e} \tag{2.12}$$

Anisotropic parameters

With an assumption of associated flow rule and one-dimensional loading, the initial inclination, α_0 and the relative rate of surface rotational hardening, ω_d of the yield curve for normally consolidated or lightly overconsolidated clay can be expressed

as[37]

$$\alpha_0 = \frac{\eta_{K0}^2 + 3\eta_{K0} - M_c^2}{3}$$
$$\omega_d = \frac{3}{8}\left(\frac{4M_c^2 - 4\eta_{K0}^2 - 3\eta_{K0}}{\eta_{K0}^2 - M_c^2 + 2\eta_{K0}}\right) \tag{2.13}$$

Where, $\eta_{K0} = 3(1 - K_0^{NC})/(1 + 2K_0^{NC})$ and $M_C = 6\sin\phi'_{cv}\ /(3 - \sin\phi'_{cv}\ )$.
The absolute rate of rotational hardening, ω depends empirically on α_0, λ^*, M and ω_d [20] according to the equation below.

$$\omega \approx \frac{1}{(\lambda_i^* - \kappa^*)} \ln\left(\frac{10M_c^2 + 2\alpha_{K0} * \omega_d}{M_c^2 + 2\alpha_{K0} * \omega_d}\right) \tag{2.14}$$

Creep parameters
Viscous parameters of the Creep-SCLAY1S model are reference time τ and intrinsic modified creep index, μ_i^*. τ depends on the incremental loading rate in the oedometer test that used to define the apparent preconsolidation pressure, σ_{po}. μ_i^* is derived from the strain vs time figure 2.9 when no bonding is present.[14]

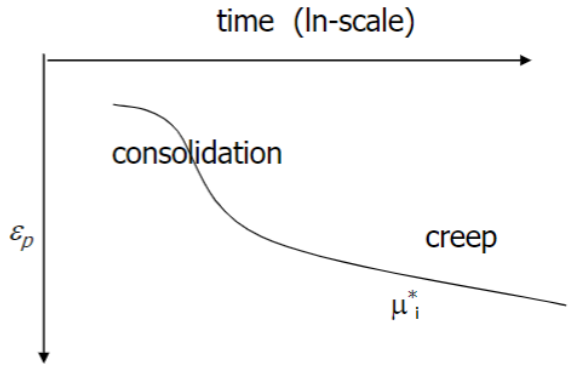

Figure 2.9: Strain vs time curve from oedometer test to define μ_i^*

Destructuration parameters
Creep-SCLAY1S considers three parameters for destructuration that are initial bonding, χ_0; absolute rate of destructuration, a; relative rate of destructuration, b. Initial bonding depends on the sensitivity of the soil and can be calculated by $\chi_0 = S_t - 1$. a and b are needed to be calibrated from laboratory tests like isotropic triaxial test by a trial and error method to get the values within a suitable range. Karstunen et al. [14] suggested ranges for these parameters, For "b" the range is between 0 and 1. For Scandinavian clays the suggested range is $0.2 < b < 0.4$. For "a" value the range is 8-12.

2.4.2 Hardening Soil model

Description

The Hardening Soil (HS) model[30] is being formulated to capture the soil behavior more accurately than other models such as Cam-Clay model, Duncan-Chang model, etc. It is an elasto-plastic model that can compute an acceptable collapse load in the plastic range. Plasticity theory, soil dilatancy is included in this model. Also, a volumetric cap yield surface is been launched which has a different shape than other soft soil models. Two different types of hardening (shear hardening and compression hardening) are considered. Permanent strains because of primary deviatoric loading are modeled by shear hardening and compression hardening handles the plastic strain due to compression loading and isotropic loading.
OCR or POP determines the initial size of the cap surface and the primary size of the shear hardening cone depends on K_0^{NC}. The cap surface swells proportionally to plastic strains. Associated flow rules are assumed for the cap surface whereas for the cone yield surface and the failure surface, non-associated flow is considered. Figure 2.10 shows the yield surfaces of the Hardening Soil model.

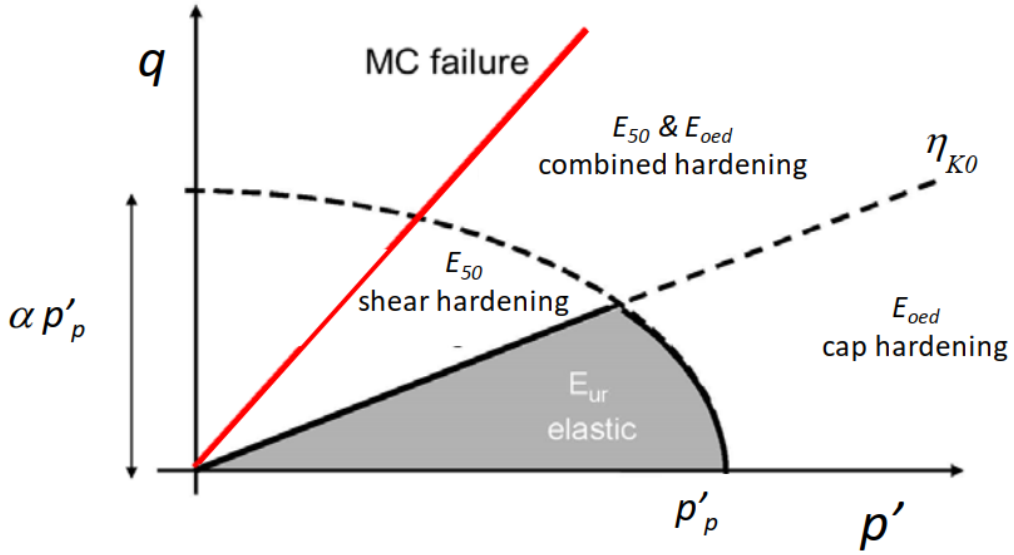

Figure 2.10: Yield surfaces of the Hardening soil model [14]

Parameters
Soil Stiffness in this model is stress-dependent. Three stiffness parameters, primary shear stiffness E_{50}^{ref}, primary compression stiffness E_{oed}^{ref} and unloading-reloading stiffness E_{ur}^{ref} and a stress dependency power, m are considered in the model. The following non-linear equation is used to define the stiffness.

$$E_i' = E_i^{ref} \left(\frac{\sigma_i + c' \cot \varphi'}{P_{ref} + c' \cot \varphi'} \right)^m \tag{2.15}$$

Where the apparent effective cohesion, c' is zero and m=1 for soft clays. For sand m = 0.5. For soils in between clay and sand, m value varies between 0.5 and 1.0.
The parameters E_{50}' and E_{ur}' can be calculated by the cell pressure, σ_3' of a tri-axial

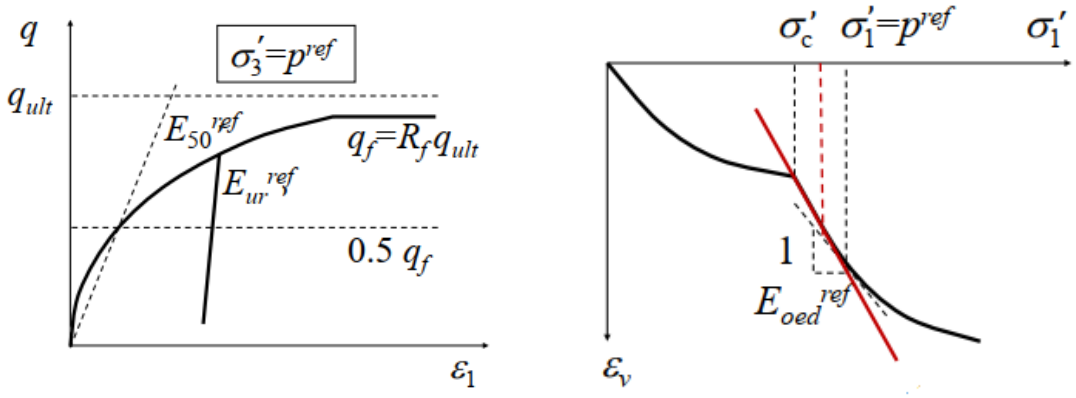

(a) Triaxial test **(b)** Oedometer test

Figure 2.11: Moduli of Hardening Soil model [14]

drained test using the equations below.

$$E'_{50} = E_{50}^{ref}\left(\frac{\sigma'_3}{P_{ref}}\right)$$
$$E'_{ur} = E_{ur}^{ref}\left(\frac{\sigma'_3}{P_{ref}}\right) \tag{2.16}$$

E_{50}^{ref} and E_{ur}^{ref} are the stiffness at a reference stress P_{ref} and can be calculated from the stress-strain curve of a triaxial test(Figure 2.11(a)). The secant modulus, E_{50}^{ref} is determined at 50% mobilization of the maximum shear strength, q_f.

The tangential oedometer modulus E_{oed}^{ref} is determined at NC range from oedometer test using the following equation.

$$E'_{oed} = E_{oed}^{ref}\left(\frac{\sigma'_1}{P_{ref}}\right) \tag{2.17}$$

Where σ'_1 is the effective vertical stress in the oedometer test.
Poisson's ratio for unloading reloading, μ_{ur} is taken as 0.2. To include the dilatancy of soil under MC failure, the model includes dilatancy angle, ψ that is calculated based on initial void ratio, e_0 of the soil and the maximum void ratio, e_{cv} at critical state.

3
Methodology

Dry deep mixing of lime-cement (LC) columns in the passive zone (the soil inside the excavation) of a deep excavation is used together with a conventional braced sheet pile wall retaining structure within the contract E02 central station of the västlänken railway tunnel project [41]. This is an ongoing project and field measurements are done continuously on the site with a trained survey team. Also, inclinometers are installed on the sheet piles of the excavation to monitor the ground movement and settlements. Site investigation data (water content, sensitivity, density, liquid limit etc) are also available which was conducted prior to the design of the whole project. Laboratory tests that are done on undisturbed clay and LC samples are CRS, triaxial test on the active and passive side (drained and undrained), oedometer test, direct shear test etc. Soil properties are calculated from site investigation data.
The scope of this master's thesis is to simulate the field condition of the deep excavation using a FE model (PLAXIS 2D). In the model, clay will be modelled with a soft soil creep model (Creep- SCLAY1S). The lime-cement composite will be modelled using Hardening Soil model and the results of the simulation will be compared with the field measurement to identify the stiffness parameters that best fit with it. Lateral movements of the retaining wall and forces on strut in the model will be analyzed and compared with the field observations. Displacement of the top soil layer and excavation bottom, Shear forces and bending moments of the retaining walls will be analyzed.

3.1 Västlänken E02 project

The västlänken project consist of eight kilometers double railway route of which six kilometers are tunnel beneath the heart of the city. Four kilometers of the tunnel will be built in rock and two kilometers will be in Gothenburg clays. Three types of tunnel are proposed, rock tunnel, concrete tunnel in rock and concrete tunnel in clay. The project has four contracts: E02 - Centralen, E03 - Kvarnberget, E04 - Haga and E05 - Korsvägen (Figure 3.1). E02 - Centralen project is all total 1800 m long of which 1700 m is on clay. It consists of a bridge, 300 m train track, 900 m tunnel and 600 m underground station pointed as 1 and 2 in Figure 3.1. The architecture of this zone differs from industrial buildings to traditional buildings in the city center.[41]

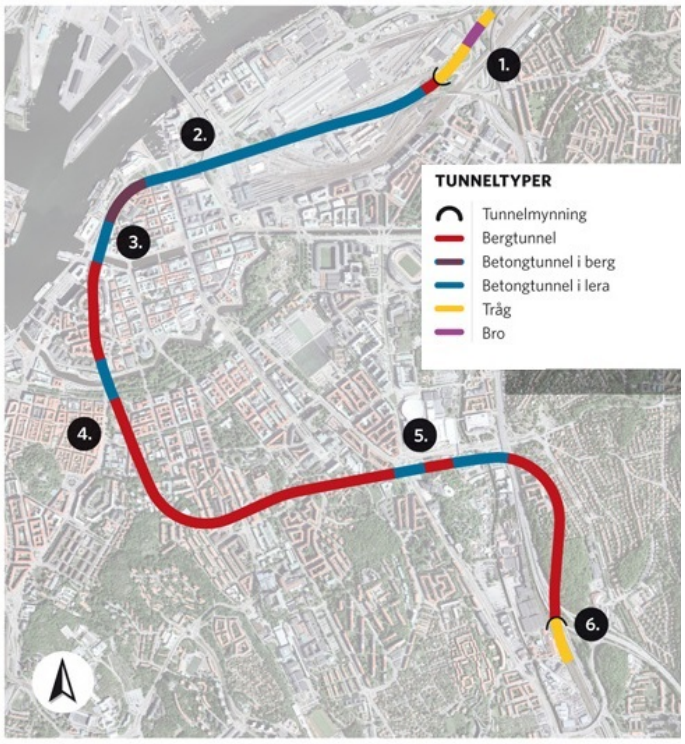

Figure 3.1: Route of the Västlänken project [36]

Construction of the tunnel in clay requires deep excavation and for that lime-cement column has been used to stabilize the clay soil in the passive side of the excavation. The effect of installing lime-cement columns in the passive side of a deep excavation will be investigated in this paper.

3.2 Site descriptions

For this study, a section near the mark 456/760 is chosen as the inclinometers are installed in this sector before the construction started (Figure 3.2). This particular section is 20 m wide and 13.5 m deep.

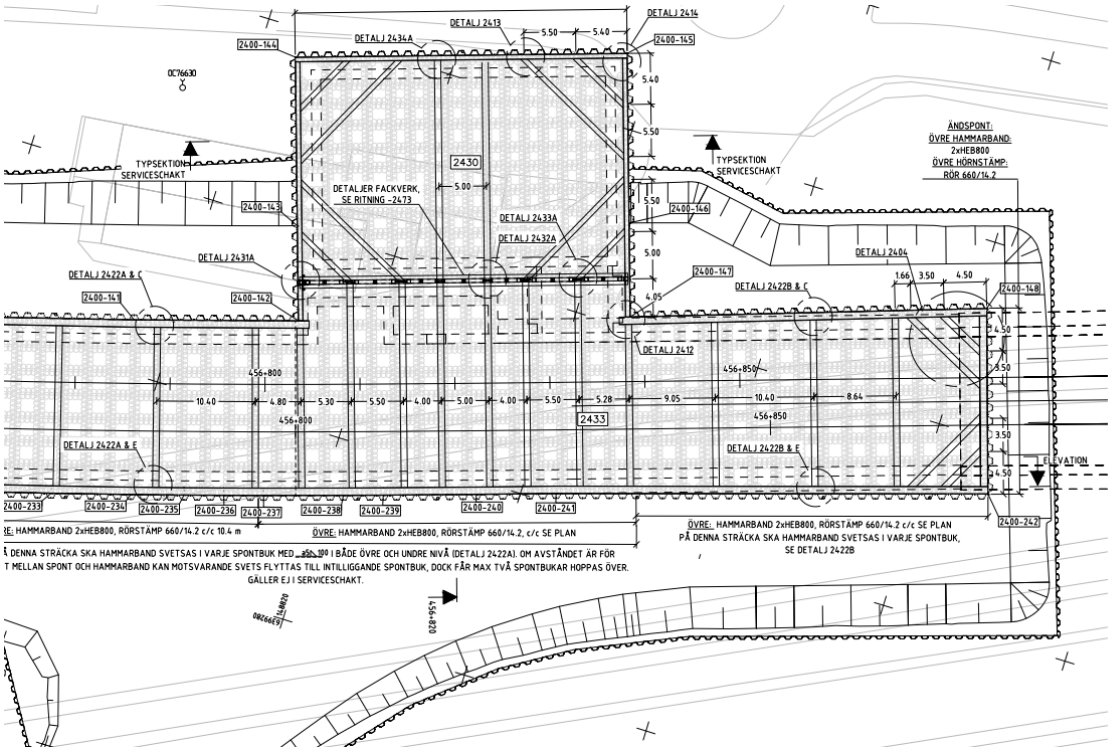

Figure 3.2: Plan of the project (Datum=0).

3.2.1 Material properties

Soil samples are collected from the site at different depths to find out the soil properties. Laboratory tests performed on the samples are CRS, direct shear test, oedometer test, triaxial drained, and undrained test. Apart from that, site investigation is done to define the index properties of soil. Figure 3.3 shows the properties of soil at various depths.

In 2016 Tara Wood [39] investigated the soil around the site and characterized the soil in various depths according to their properties. Figure 3.5 shows the variations of the undrained shear strength of the soils at different layers. The soil consists of 2-3 m filling layer above 70 m clay with an undrained shear strength of 18 kPa + 1.7 kPa/m from 5 m depth. This soil profile is originated by long term sedimentation of the Göta river during the glacial and post-glacial period. In table A.1, the initial state of soil is given according to Tara Wood [39].

The lime-cement column is injected in the passive side of the excavation with an area coverage ratio of around 65%. A general grid of the lime-cement and picture of the construction site with the boundary between the stabilized and unstabilized clay is shown in figure 3.4. Triaxial compression and extension tests and oedometer tests are done on the lime-cement columns. Samples of these tests are collected from the construction site and also prepared at lab mixing lime-cement with soil. The unit weight, friction angle, and cohesion of the LC columns are derived from laboratory tests approximately 18 kN/m^3, 35^0 and 10 kPa. The triaxial test results are shown in figure A.2 and A.3.

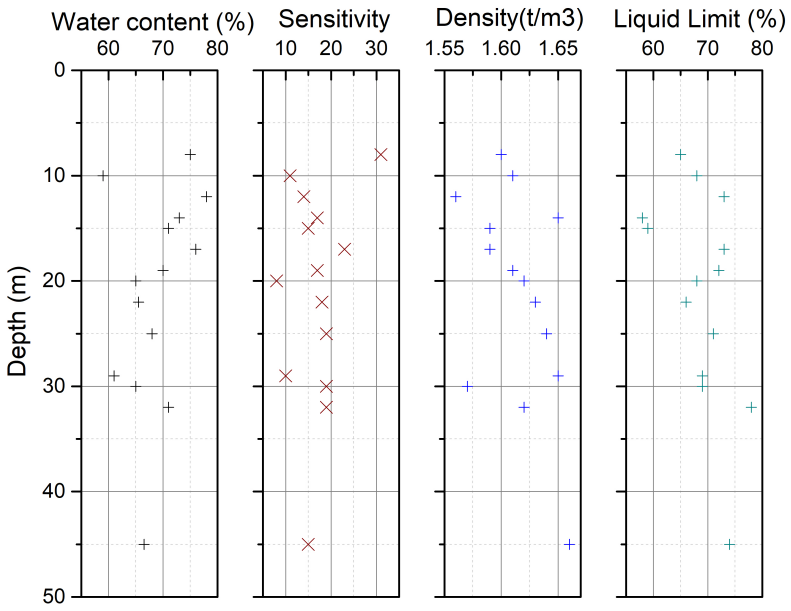

Figure 3.3: Variations of Water content, Sensitivity, Density and Liquid limit with depth

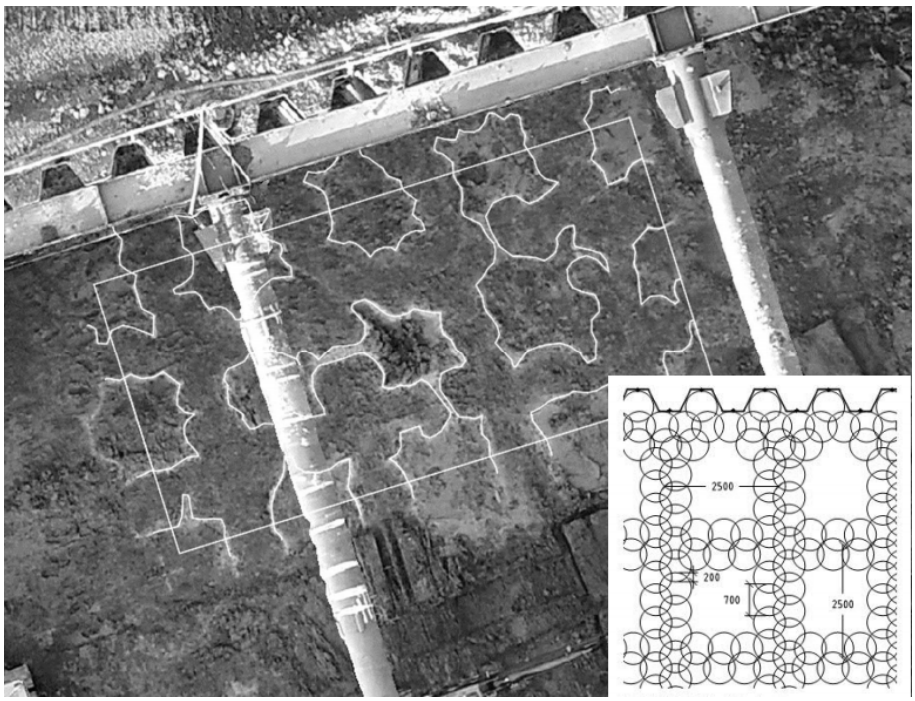

Figure 3.4: Top view of the excavation at level -7 where lime-cement stabilized soil is marked [41]

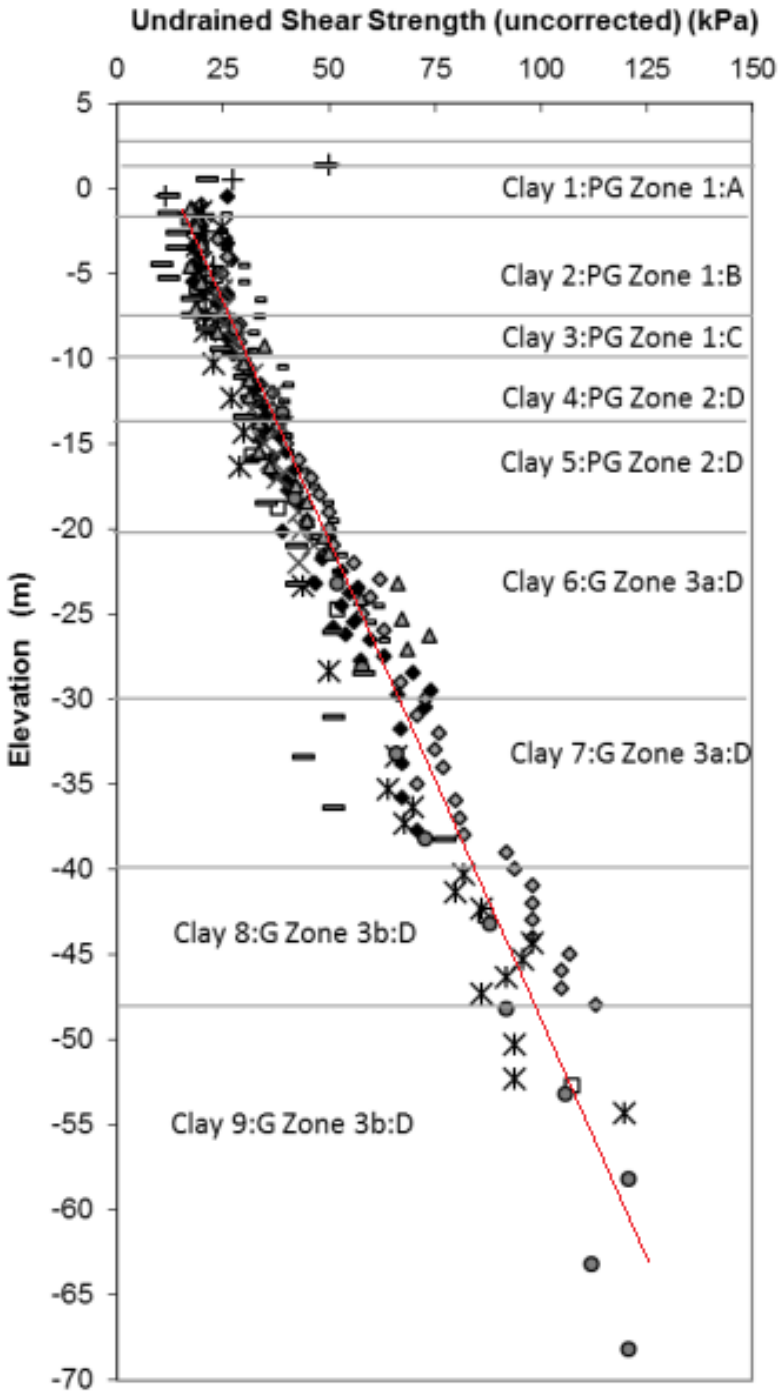

Figure 3.5: Ground profile for Gothenburg, and uncorrected field vane profiles(PG= post Glacial, G=Glacial) [39]

3.2.2 Geometry

The section analyzed in this study is presented in figure 3.6). The excavation is almost 13.5 m deep and 20 m wide.

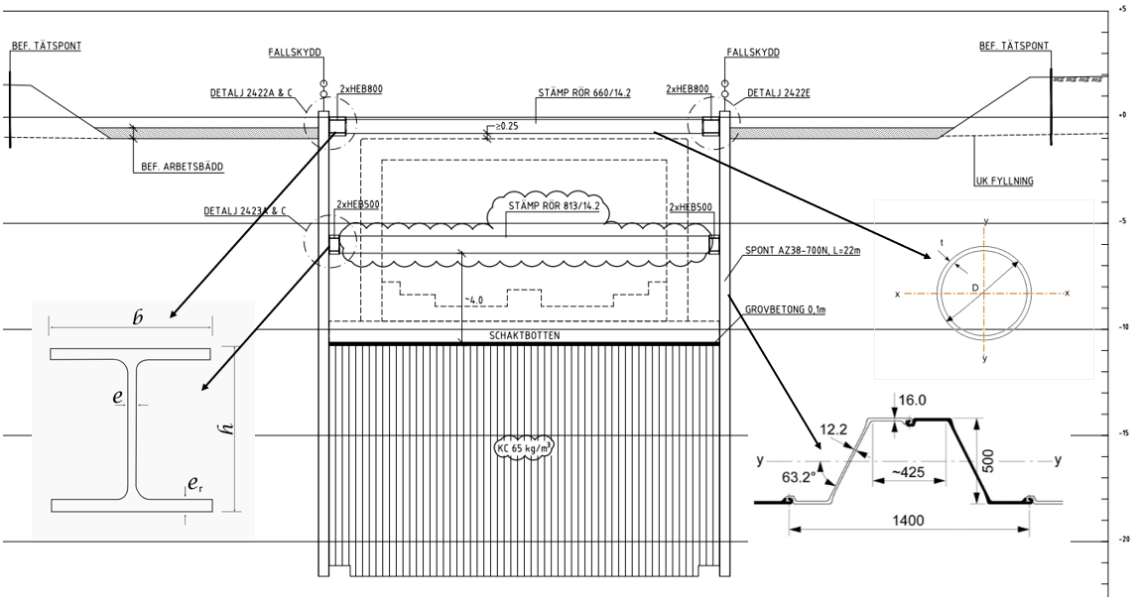

Figure 3.6: Section 456/760 of the project

Sheet piles are used as a retaining structure of the excavation, struts in two different levels are used to provide lateral stability of the whole system. Sheet pile used in this project is AZ38-700N. Sectional dimensions are shown in figure 3.6 and properties are provided in table A.2. The length of the sheet pile is 22 m.
Two struts levels are used in the structural system to support the vertical sheet pile wall. The top and the bottom struts are installed at level 0 and level -7 respectively. Strut spacing varies in different sections. Spacing between the struts at the top and the bottom level is shown in figure 3.2 & A.1. Hollow circular sections of 14.2 mm thickness are used as the strut. The radius of the struts in the top and the bottom level is 660 mm and 813 mm respectively. The sectional properties of the section are provided in table A.3. Correspondingly, two HEB-800 and HEB-500 beams are used throughout the sheet piles to support the struts at the top and the bottom level. Sectional properties of the beams are provided in table A.4.
At the bottom of the excavation 200 mm concrete working platform is cast prior to the 500 mm thick concrete plate for the tunnel.

3.2.3 Excavation stages

The excavation was started with the excavation of the top 2 m fill till datum 0 m. Then the 20m long sheet piles were installed. The passive zone (the soil inside the excavation) of the excavation was then stabilized with lime-cement columns with an area ratio of 65% down till the bottom elevation of the sheet pile. The amount of admixture is changed from 40 kg/m^3 to 80 kg/m^3 for the excavated soil and the soil that remained below the bottom of the excavation. After that, excavation was done up to -2 m and the upper-level struts were installed on datum 0 m. Then the excavation was continued till -7.2 m and the bottom struts were installed at level -7 m. The excavation was then carried out till -11.2 m. After that, a temporary coarse concrete slab of 0.2 m was cast following the casting of a permanent concrete slab of 1 m for the bottom of the tunnel. Aftet the concrete had hardened the lower strut level was dismantled.

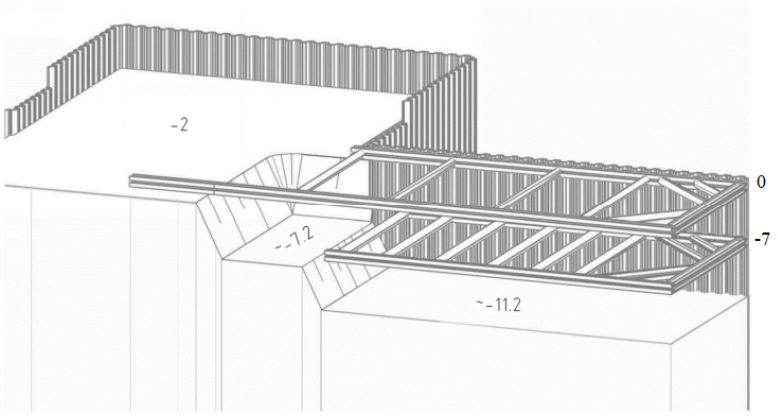

Figure 3.7: 3D model of the section [41]

Construction sequences or the erection with an end date of every phase are provided in table 3.1.

Table 3.1: Construction phases with end date

Phases	**End date**
Starting of the excavation of fill	2019-02-01
Finished the excavation of fill	2019-04-09
Excavation till level -2	2019-09-25
Installation of upper struts	2019-10-07
Excavation till level -7	2019-10-17
Installation of bottom struts	2019-11-03
Excavation till level -11.2	2019-11-24
Casting of temporary concrete slab	2019-11-24
Casting of permanent concrete slab	2019-12-12
Dismantling the bottom struts	2020-01-15

3.2.4 Field measurements

Figure 3.8 shows the plan view of the site along with the positions of the measuring devices installed. Six inclinometers are installed in the project, among them Ink2433-4 and Ink2433-5 automatically measures the ground movements. The dotted line on figure 3.8 shows the positions of the two inclinometers which provide data up to 35 m depth from the ground surface. Figure 3.9(a-f) show the horizontal displacements measured by the two inclinometers as the excavation progresses. Initially, the movements were outward which means the retaining walls were pushed largely by the pressure from the passive composite materials (LC columns and soil mixture). The maximum outward movement of the sheet pile wall was recorded after the installation of the LC columns and was around 47mm at the depth between 11 m and 15 m. As excavation work progresses the retaining wall moves inward because of the pressure of the active soil.

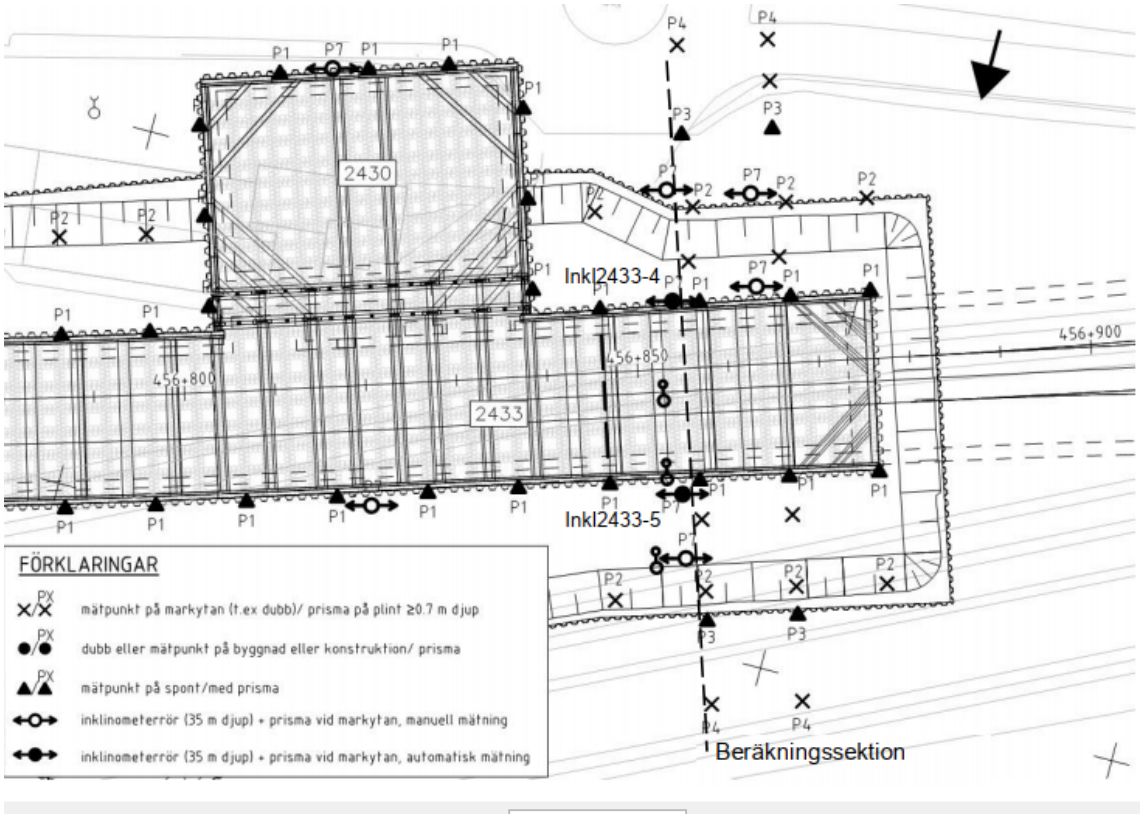

Figure 3.8: Instrumentation setup of the project [41]

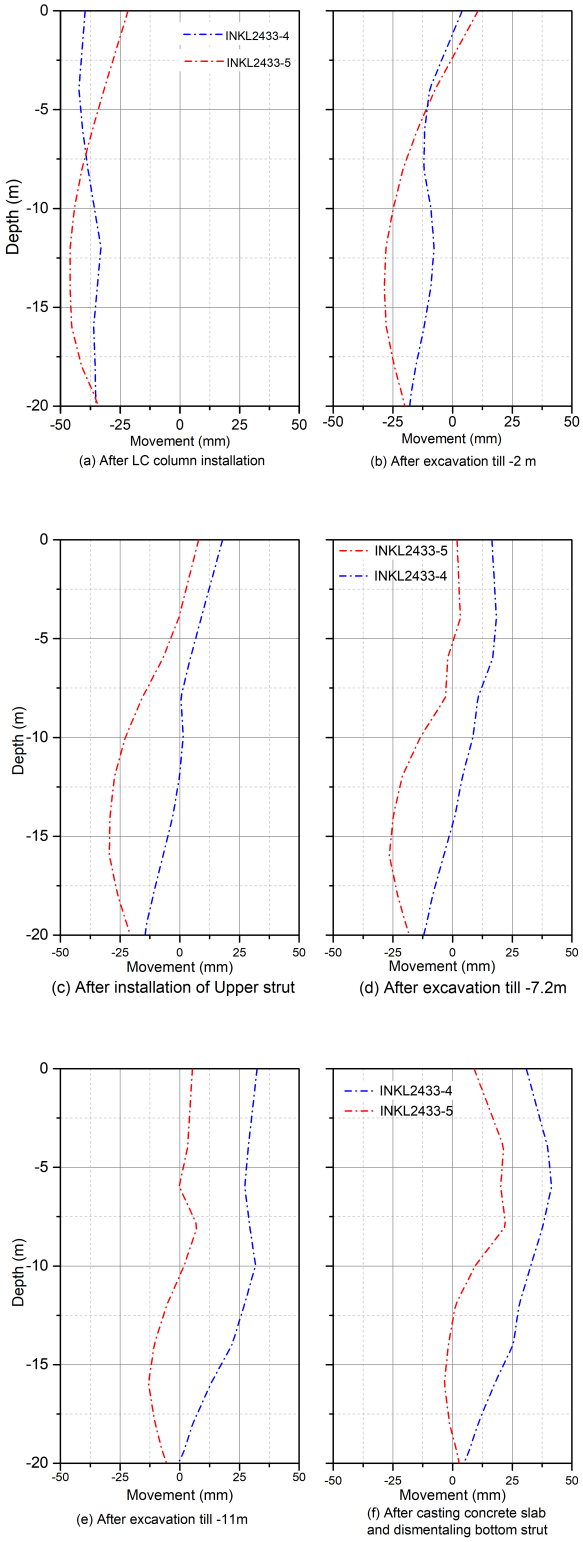

Figure 3.9: Movements of the inclinometer at various stages of construction [Positive= inward, Negative= outward]

Development of the axial loads with time are shown in figure 3.10 and figure 3.11. In figure 3.10, the forces at the upper strut level during the construction process are presented. Sensors that collect the data are installed in the middle and 3 m from one end of strut 2.
Initially, the strut force is around 1700 to 1900 kN and starts reducing after the installation of the bottom struts. Axial loads reduced to 1000 kN approximately after casting the permanent slab. When the bottom strut disassembled, loads on top struts increases again to around 2100 to 2400 kN.

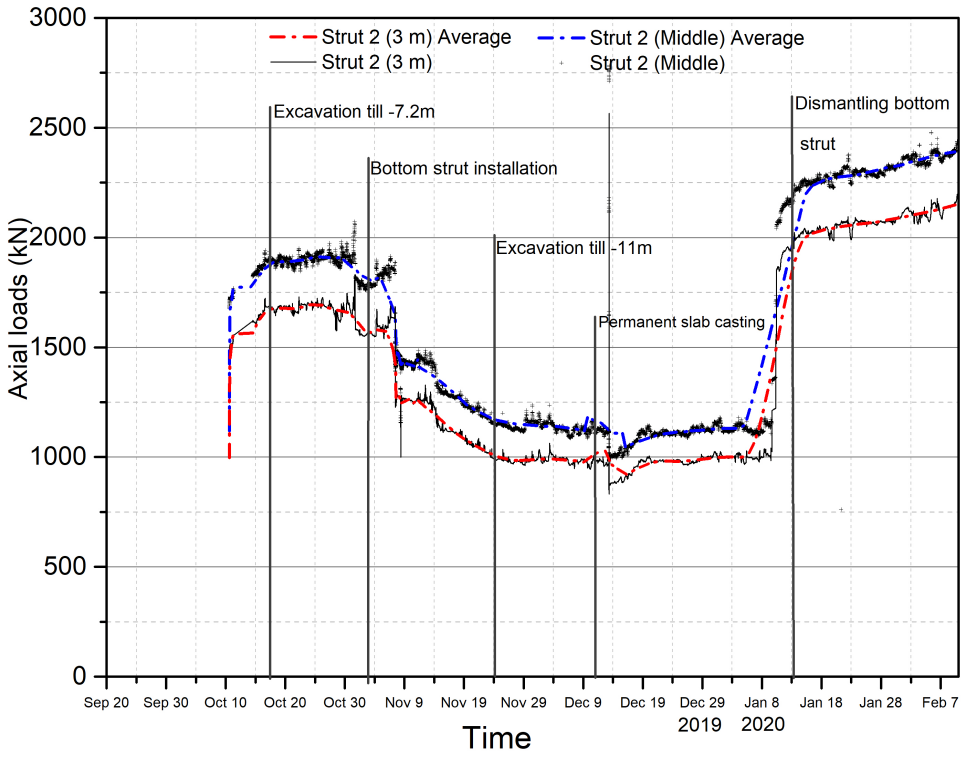

Figure 3.10: Development of the top strut forces during the excavation process

Figure 3.11 shows the forces in the bottom strut at various construction stages. The data are collected from a sensor installed at a distance of 3 m from one end of strut 3. Loads on the bottom slab remain almost constant to 1700 kN throughout the construction stages.

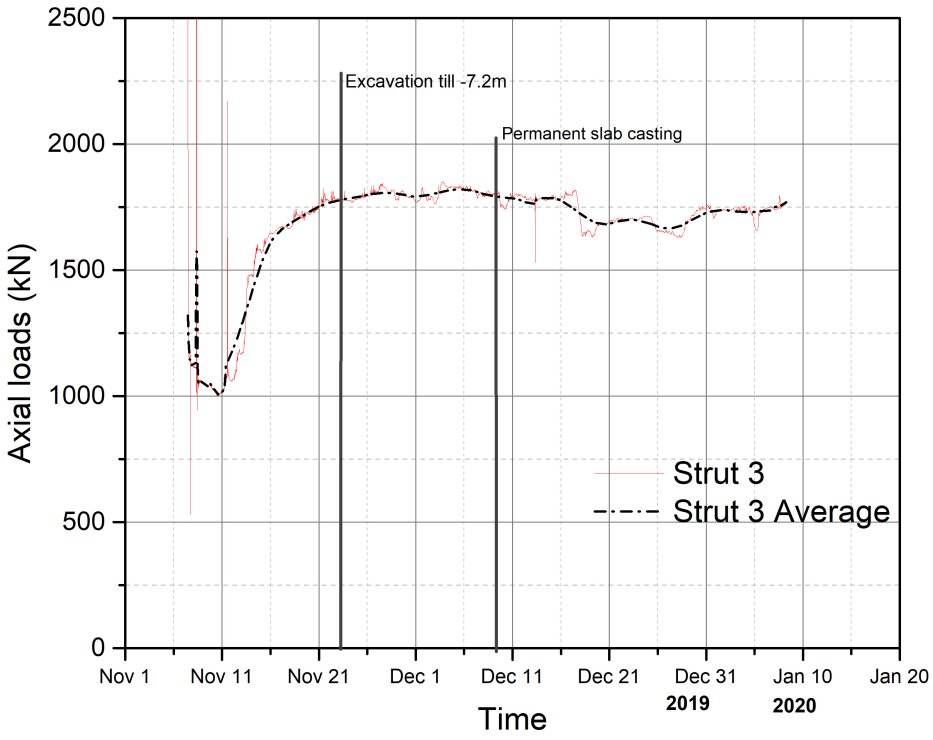

Figure 3.11: Development of the bottom strut forces during the excavation process

3.3 Numerical model for the Västlänken E02 project

A numerical model is developed using PLAXIS 2D 2019 version. Creep-SCLAY1S and Hardening soil model is utilized to represent clay and line-cement columns respectively.

3.3.1 Geometry

The soil layering consist of a 2 m fill at the top and nine different clay layers as shown in figure 3.12. The model created is 100 m in the horizontal and vertical direction. The elements of the model are 6-noded. As the excavation is symmetrical around Y-direction, the created model has a symmetrical boundary in min x-direction. The max x-direction and min y-direction boundary are fixed and the max y-direction boundary are free in the model. The mesh used in the model is shown in figure A.4.

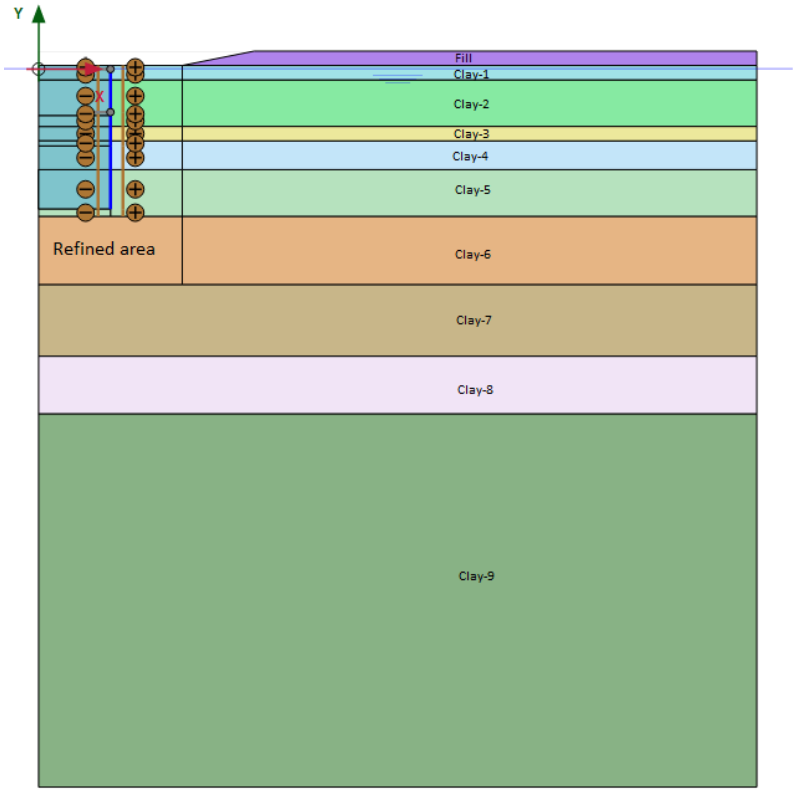

Figure 3.12: Geometry of the model

Very fine mesh is considered with a refined area near the excavation zone. The total elements in the model are 55162 and the total nodes are 111377.

3.3.2 Model parameters

The clay layer 1 to 9 is modelled using the CREEP-SCLAY1S model. The Hardening Soil model is utilized to model lime-cement composite and the fill in the top. Undrained-A type of drainage is considered for the calculation. Parameters used for

clay are shown in table 3.2. Bold parameters in table 3.2 are calculated from the lab test results on samples collected from the construction site.

Table 3.2: CREEP-SCLAY1S model parameters [39]

Parameters	Clay 1	Clay 2	Clay 3	Clay 4	Clay 5	Clay 6	Clay 7	Clay 8	Clay 9
κ^*	0.032	0.025	0.018	**0.023**	**0.015**	**0.009**	**0.015**	**0.024**	**0.024**
κ^*_{ss}	0.0029	0.0048	0.0041	0.0045	0.0044	0.0048	0.0049	0.0049	0.0051
υ	0.15	0.15	0.15	0.15	0.15	0.15	0.15	0.15	0.15
λ^*_i	0.09	0.09	0.09	**0.11**	**0.051**	**0.047**	**0.0748**	**0.13**	**0.13**
M_c	1.4	1.55	1.6	1.6	1.6	1.35	1.3	1.23	1
M_e	1.2	1.15	1.15	1.15	1.15	1.1	1.1	0.9	0.95
ω	120	100	100	100	100	110	110	100	100
ω_d	0.3	0.1	0.1	0.1	0.1	0.2	0.2	0.2	0.2
ξ	9	12	12	12	12	12	12	12	12
ξ_d	0.2	0.4	0.4	0.4	0.5	0.2	0.2	0.2	0.2
e_0	1.4	2.1	2.1	1.71	1.8	1.57	1.74	1.65	1.55
α_0	0.5	0.7	0.7	0.7	0.7	0.35	0.35	0.4	0.4
χ_0	10	8	9	8	6	9	8	8	8
τ	1	1	1	1	1	1	1	1	1
μ^*	0.003	0.003	0.004	0.0033	0.0028	0.0022	0.0022	0.0018	0.0034
OCR	2	1.65	1.3	1.29	1.22	1.16	1.14	1.14	1.35

For the lime-cement columns, different stiffness values are considered. The initial stiffness are the average values from the 12 triaxial test data conducted on the lime-cement composite samples shown in table A.5. These samples are the mixture of lime and cement and to originate the field raio of lime-cement (65%) and clay (35%) trial and error of the stiffness parameters are conducted to get the best fit with the measured data, the reduced stiffness set are taken into account. The higher stiffness are considered to check the sensitivity of the model. Parameters to represent the fill and lime-cement columns are shown in table 3.3.

Table 3.3: Hardening Soil model parameters

Material	E^{ref}_{50} (MPa)	E^{ref}_{oed} (MPa)	E^{ref}_{ur} (MPa)	m
Fill	10	7	30	0.5
LC-initial stiffness	120	60	360	1.0
LC-reduced stiffness	25	15	75	0.75
LC-higher stiffness	180	100	500	0.8

Structural elements in the model are the retaining wall, the struts, and the concrete slab at the bottom of the excavation. The parameters of these components are shown in table A.6.

3.3.3 Construction sequences

The model is set up according to the actual construction sequence to represent the field scenario. Table 3.4 shows the phases considered in the model. Phreatic pore water pressure is considered in the model.

Table 3.4: Calculation phases in PLAXIS 2D

Phase	Calculation type	Total time	Description
Initial	K_0-procedure	0	-
Excavation of fill	Consolidation	31	2 m soil fill is excavated. Bottom of the fill is 10 m from actual excavation with a mild slope.
Retaining wall installation	Consolidation	70	The retaining wall is activated with the positive and negative interfaces.
Lime-cement mixture injection	Consolidation	188	The material in the passive side of the excavation is replaced by the lime-cement column material up to the depth of retaining wall.
Positive axial strain (Outward)	Consolidation	189	To simulate the increase in volume due to LC insertion this stage is introduced. Positive volumetric strain is applied till -20 m.
Negative axial strain (Inward)	Consolidation	234	To simulate the drying, shrinkage, air and pore pressure dissipation this stage is initiated.
Excavation till –2 m	Consolidation	235	Top 2 m of the LC-composite is excavated. First excavation stage.
Installation of top strut	Consolidation	247	Top strut is installed at -0.5m from top of clay layer.
Excavation till –7 m	Consolidation	257	Excavation is done till -7m from top. Second excavation phase.
Installation of bottom strut	Consolidation	274	Bottom strut is installed.
Excavation till –11.2 m	Consolidation	295	Third excavation stage.
Concrete slab casting	Consolidation	313	500 mm thick concrete slab is installed at the bottom of the excavation.
Dismantling bottom strut	Consolidation	347	Bottom strut is taken off(end phase).

To simulate the volume increase after lime-cement column installation an extra phase is introduced in the calculation. In this phase, positive axial strain is inserted in the passive area to replicate the increased volume. From ground level down to the excavation bottom an axial strain of 0.4% and below the excavation bottom till 20m a strain of 0.5% is inserted in this phase. Then, in the next phase the

drying, shrinkage, air, and pore water pressure dissipation is imitated by inserting negative axial strain in the passive zone. A negative strain of 0.15% and 0.2% are introduced above -11.2m and below the excavation bottom till 20m respectively. These variations are because of the different admixture amount inserted above and below the excavation bottom. These two stages are represented in figure A.5.

4
Results

Calculations has been performed using three different sets of stiffness for the LC material. The initial set of stiffness is the average value of all the lab tests conducted on 12 lime-cement samples. The adjusted stiffness parameters are considered after some trial and error to best-fit the field measurements. The last stiffness set is higher than the initial set to check the sensitivity of the model on stiffness parameters. Finally, a comparison among the three sets of results with the field measurement is shown and discussed.

4.1 With initial lime-cement stiffness

Retaining wall movements from the numerical simulations at various stages are compared with the measured data (figure 4.1). The red and blue dotted lines represent the measured field data from inclinometer 2433-5 and 2433-4 respectively and the black solid line represents the model prediction with different lime-cement stiffness parameters. Negative displacements represent the outward movement of the retaining wall and positive movements illustrate inward deformation towards the excavation.
After lime-cement injection, the deformation of the retaining wall is around 30 mm outward over the depth. After the first excavation till -2 m, the bottom half of the wall is moved outward around 20 mm and the top moved towards the excavation about 12 mm from the initial position. The shape of the curve is similar to the data extracted by inclinometer 2433-5. The wall does not move that much from the previous stage when the upper strut is installed in the model but after the excavation till -7 m a huge difference in the wall movement is noticed from the previous stage. The wall moved towards the excavation and the maximum movement is 25 mm at -5 m from the top. Till this stage, the model predictions follow the inclinometer data. But after the excavation till -11 m, model approximation varies from the measured data. At this stage the measured movement at the bottom of the wall is approximately zero, whereas the predicted movement is around 20 mm inward. The maximum measured displacement is 38 mm at the excavation bottom (-11 m from the top). Predicted deformation at the top of the wall is around zero which is not aligned with the inclinometer data. The deformation curve is the same after installing the concrete slab and dismantling the bottom strut.

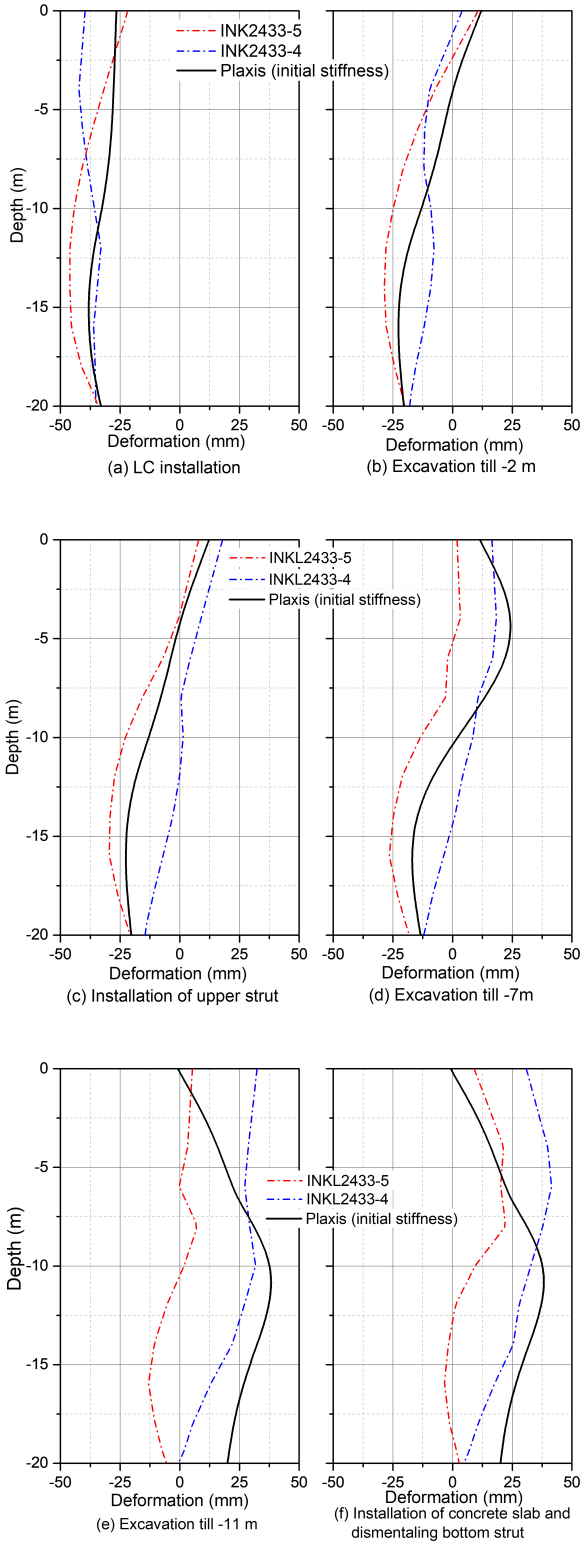

Figure 4.1: Retaining wall movements at various stages of construction [Positive= inward, Negative= outward]

The forces in the top strut can be divided into three sections. Initial forces in the top strut are around 1700 kN which reduces to 950 kN after the excavation till -11 m. Then strut force increases to 2300 kN after dismantling the bottom strut. The predicted strut forces are shown in figures 4.3 and 4.4 with the measured value. Top strut forces are well predicted by the model in the initial stages, but after excavation till -11 m the model approximation is less than the observed data. But in the end phase, the model prediction of top strut forces is well-matched with the sensor measured force. The forces in the bottom strut are over-predicted by the model. The measured force in the sensor is around 1800k kN whereas the model approximation is 2200 kN.

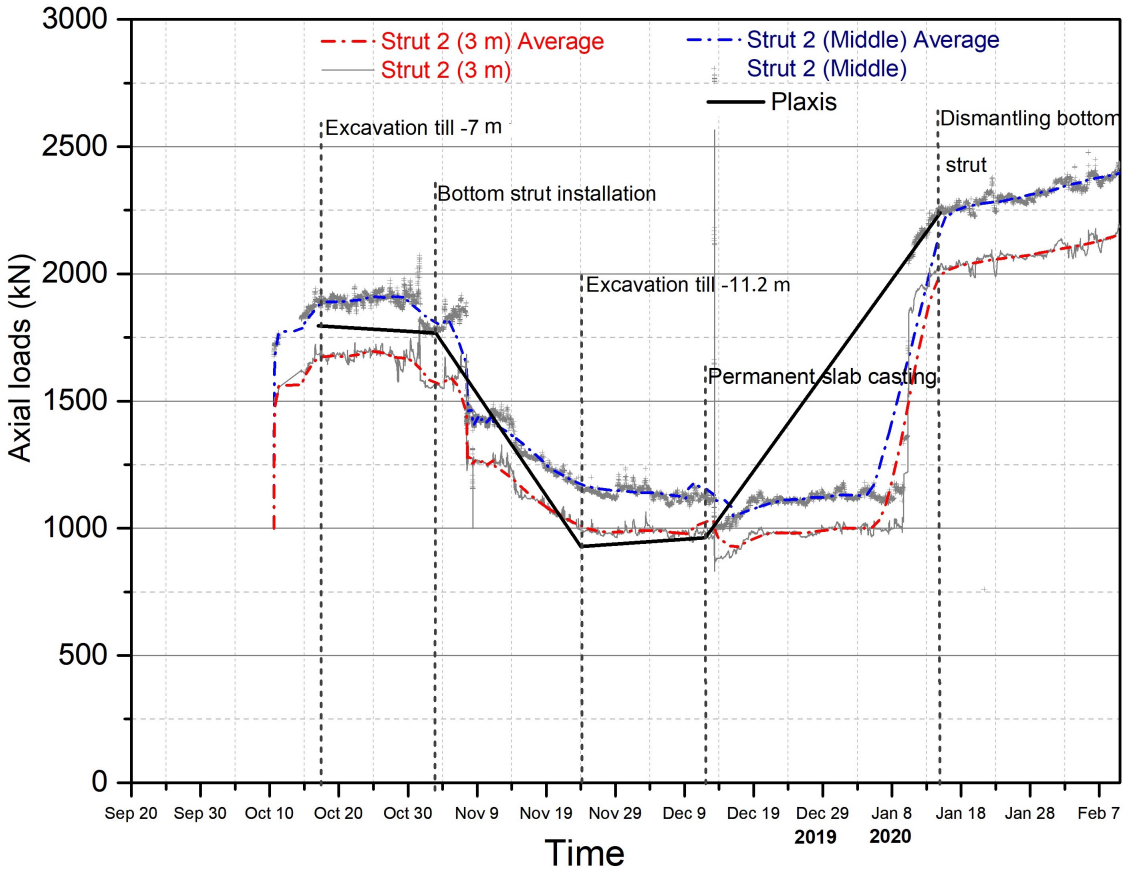

Figure 4.2: Top strut forces with initial stiffness parameters

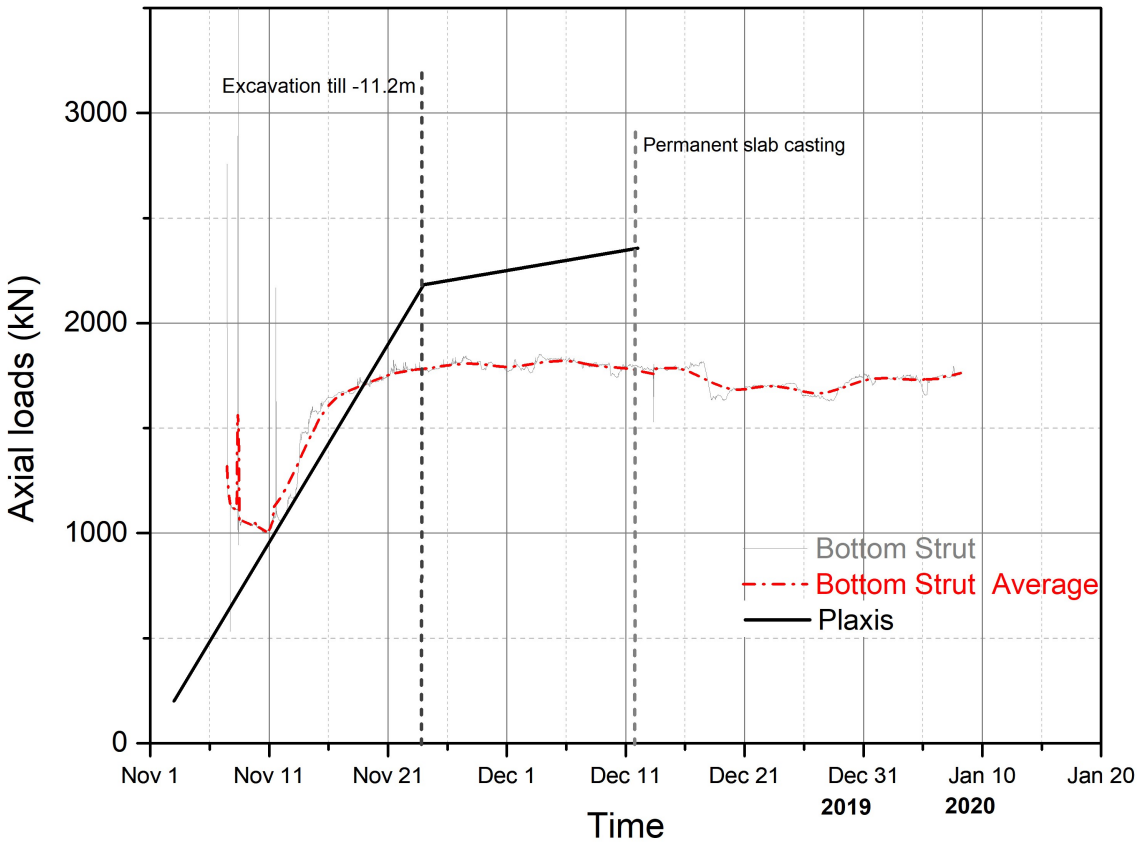

Figure 4.3: Bottom strut forces with initial stiffness parameters

Figure 4.4 shows the vertical movement of the excavation bottom at various stages. The vertical movement of the top clay layer is shown in figure 4.5. 20 m (same as the depth of the wall) in the horizontal direction from the retaining wall is taken into consideration to represent the vertical movement of the top clay layer. At the initial stages, the soil layer moved around 50 to 70 mm upward and the upward movement is around 120 mm at the later stages after excavation till -11 m. The maximum vertical settlements in this case are within the suggested range of 0.1%H (11 mm) to 10%H (1100 mm) by Moormann[23].

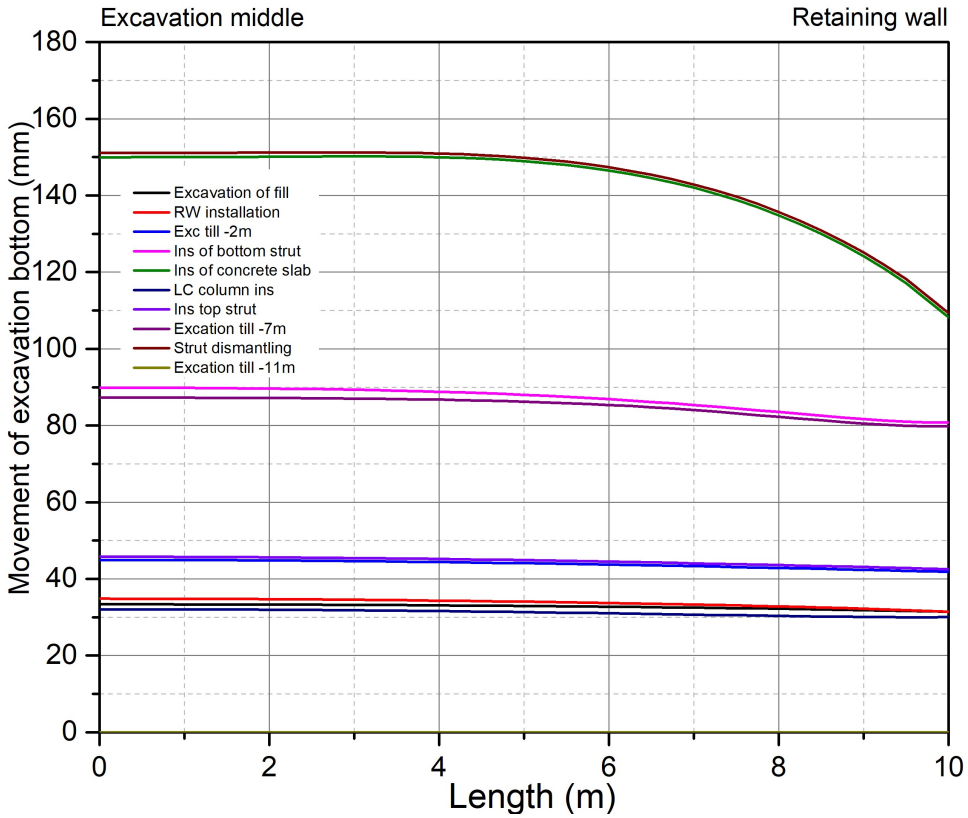

Figure 4.4: Excavation bottom displacement with initial stiffness parameters

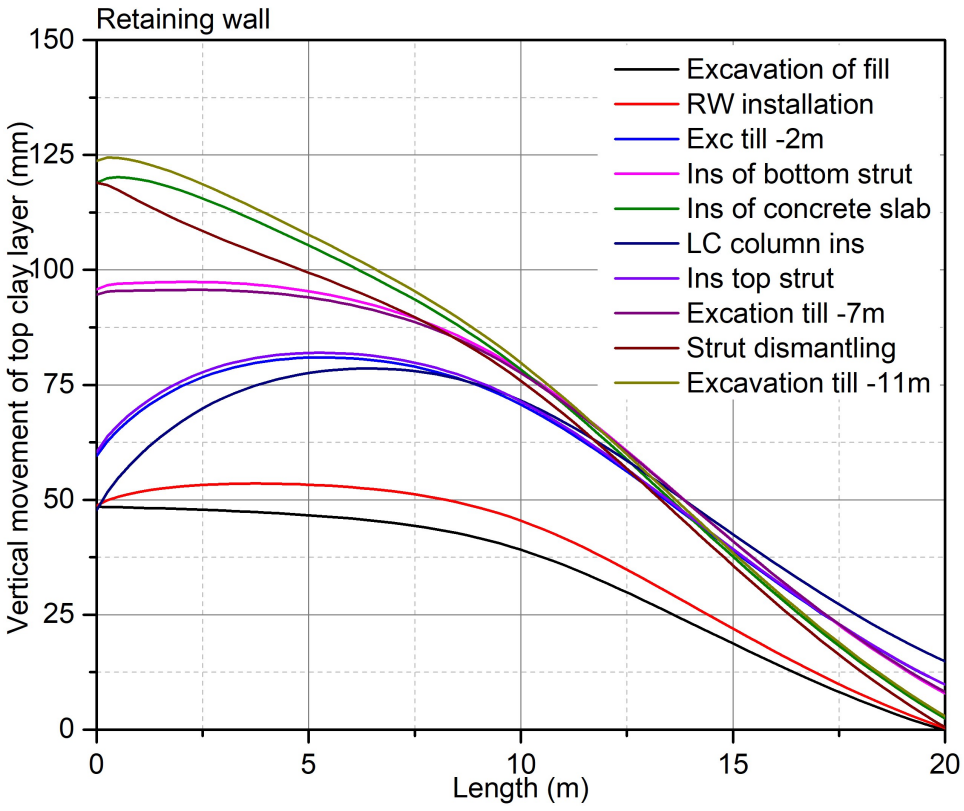

Figure 4.5: Displacement of the top clay layer with initial stiffness parameters

4.2 With adjusted lime-cement stiffness

The movements of the wall at different stages with adjusted lime-cement stiffness parameters are shown in figure 4.6. When LC is installed, the outward wall movement is around 30 mm. After the first excavation till level -2 m, the top of the wall moved towards the excavation. At the top, the displacement is around zero and at the bottom, the wall is at 15 mm outward from its origin. Displacements of the wall are similar after the installation of the upper strut. The plaxis prediction matched well with the inclinometer data in these three stages [Figure 4.6 (a), (b) & (c)]. The second excavation till level -7 m has a huge impact on the wall movement as it moves more towards the excavation zone. Maximum displacement at this stage is around 20 mm inward at a depth of 5 m from the top. Full of the wall moved inward after excavation till -11 m. The top and bottom of the wall moved around 10 mm and the maximum deformation is approximately 30 mm at the excavation bottom (-11 m). The displacement curve does not change much after the slab installation and the bottom strut dismantling. The inclinometer measurement in these stages matches well with the model prediction.

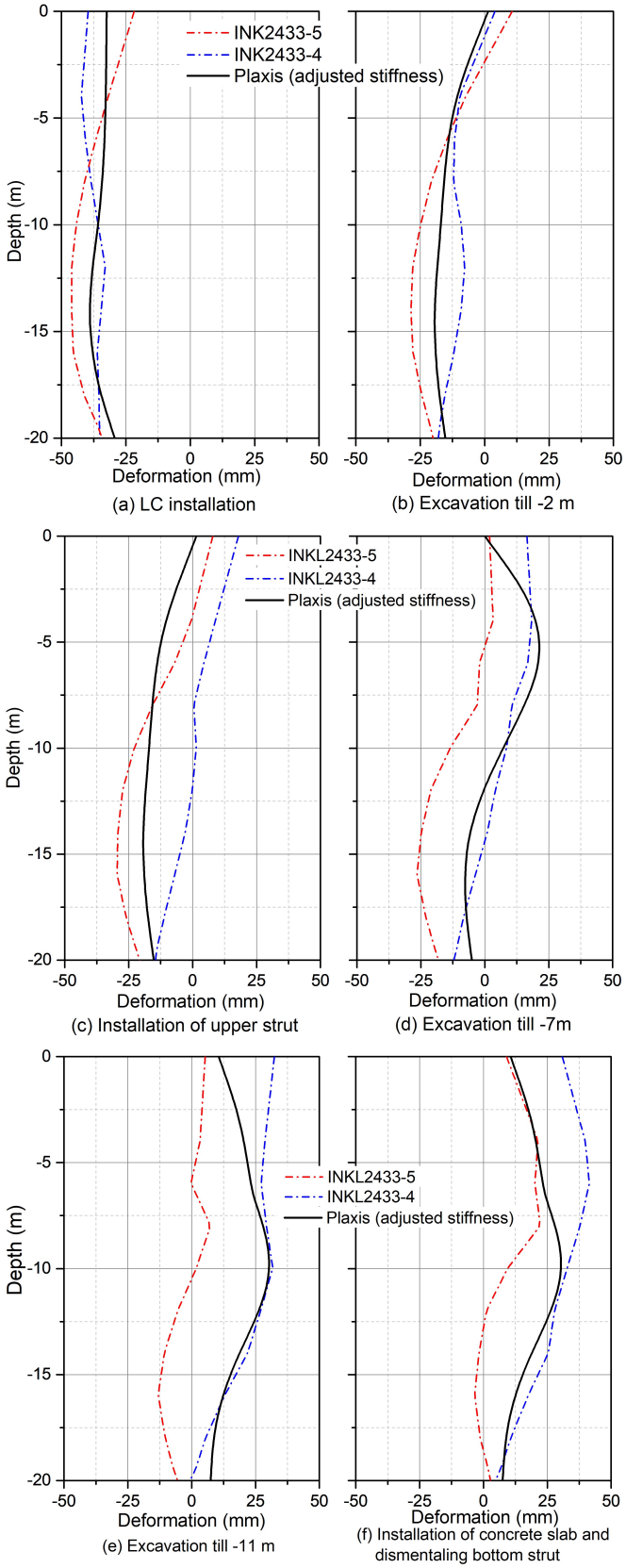

Figure 4.6: Retaining wall movements at various stages of construction [Positive= inward, Negative= outward]

The measured and predicted forces in the top and bottom struts are shown in figure 4.7 and 4.8 respectively. Overall the approximated top strut forces fitted well with the observed value, except the model over-predicted the force around 2400 kN at the end-stage.

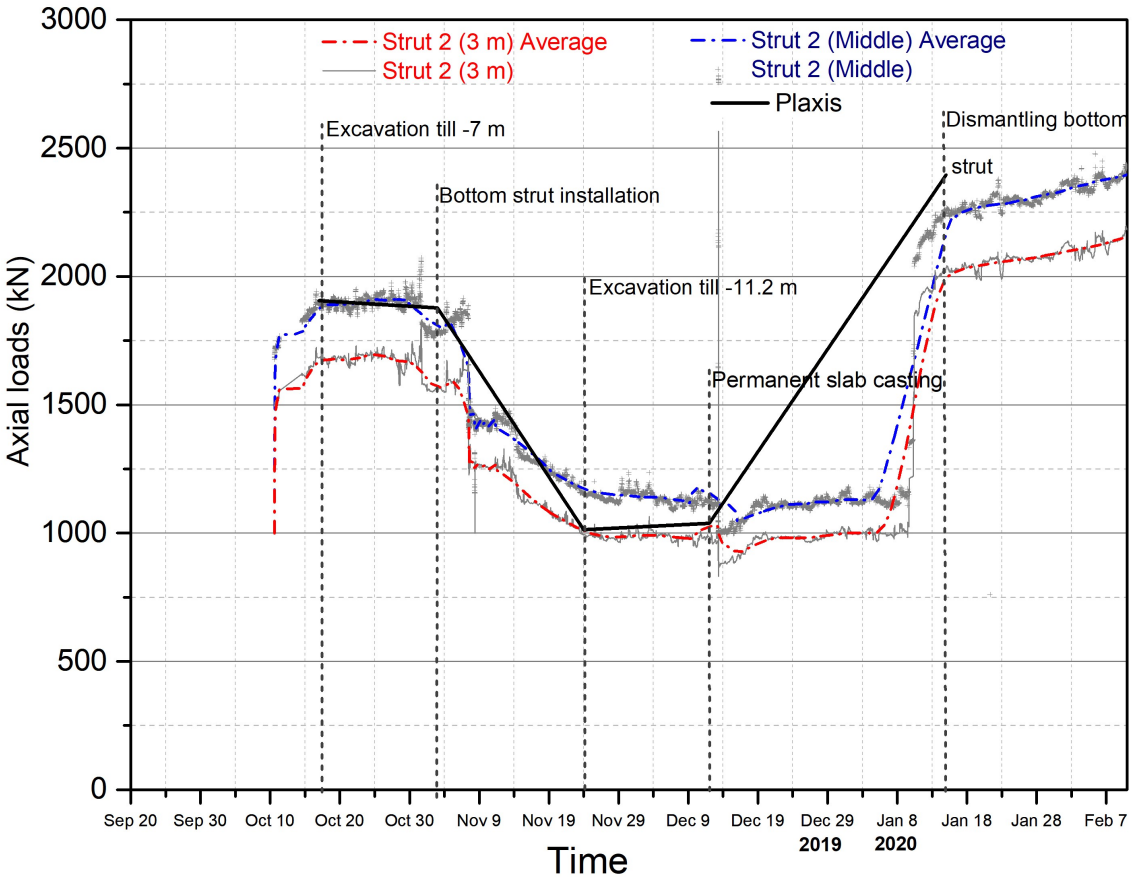

Figure 4.7: Top strut forces with adjusted stiffness parameters

The model approximation of the forces in the bottom strut is around 2800 kN whereas the field measurement is approximately 1700 kN. The model does not simulate much in the bottom force.

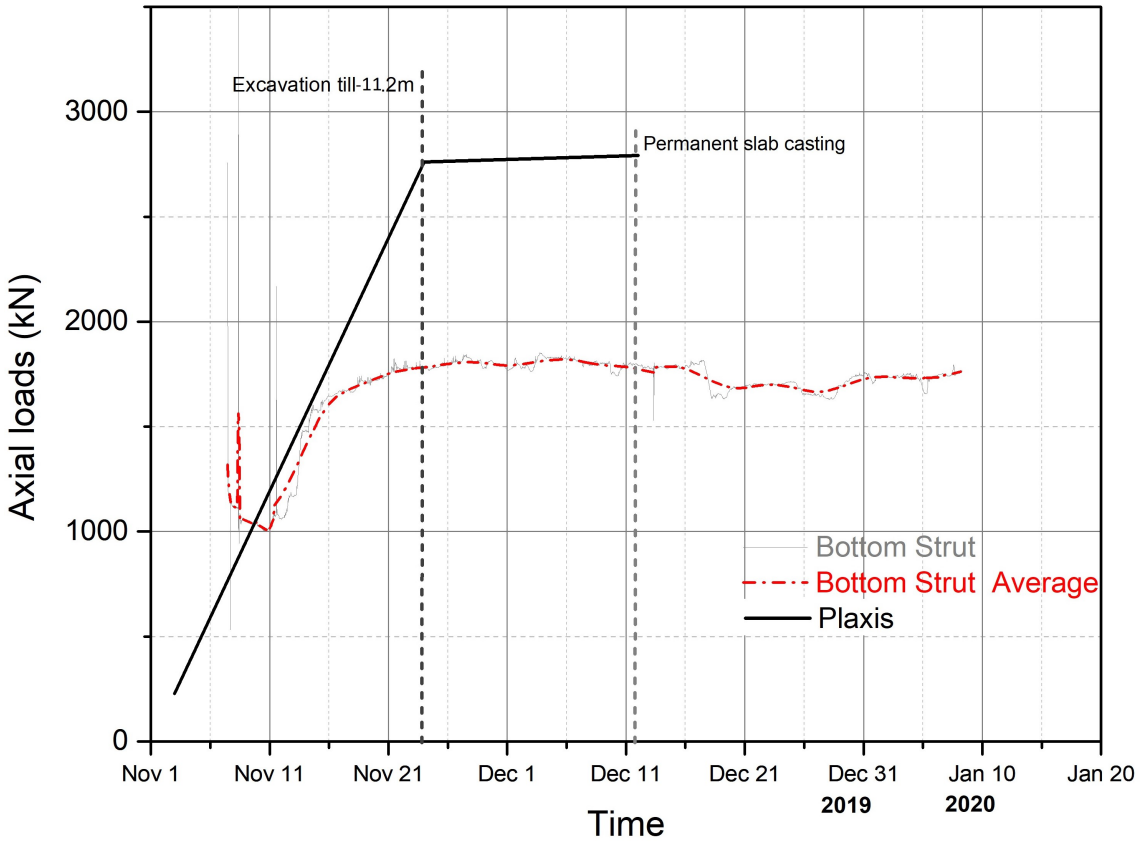

Figure 4.8: Bottom strut forces with adjusted stiffness parameters

The vertical displacement of the excavation bottom at various construction stages is shown in figure 4.9. The maximum upward movement of the bottom is approximately 170 mm at the end stages of the calculation.
Displacements of the top clay layer are illustrated in figure 4.10. Maximum vertical movement of the top soil layer is around 115 mm near the retaining wall which is within the range of 11 mm to 1100 mm suggested by Moormann [23] .

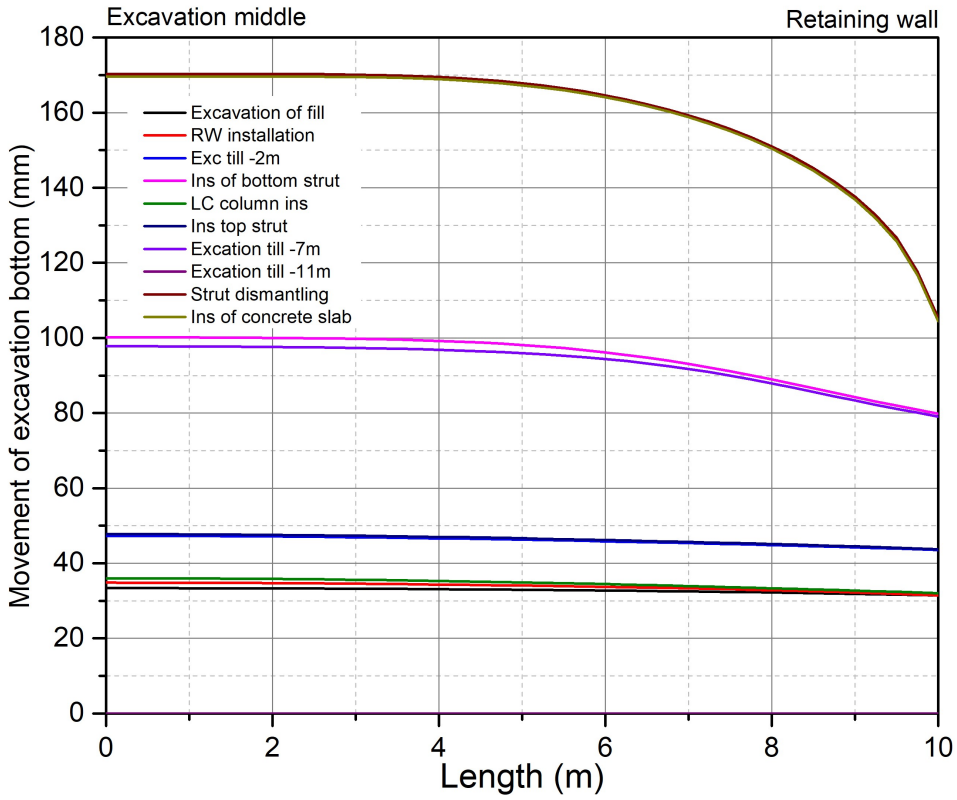

Figure 4.9: Excavation bottom displacement with adjusted stiffness parameters

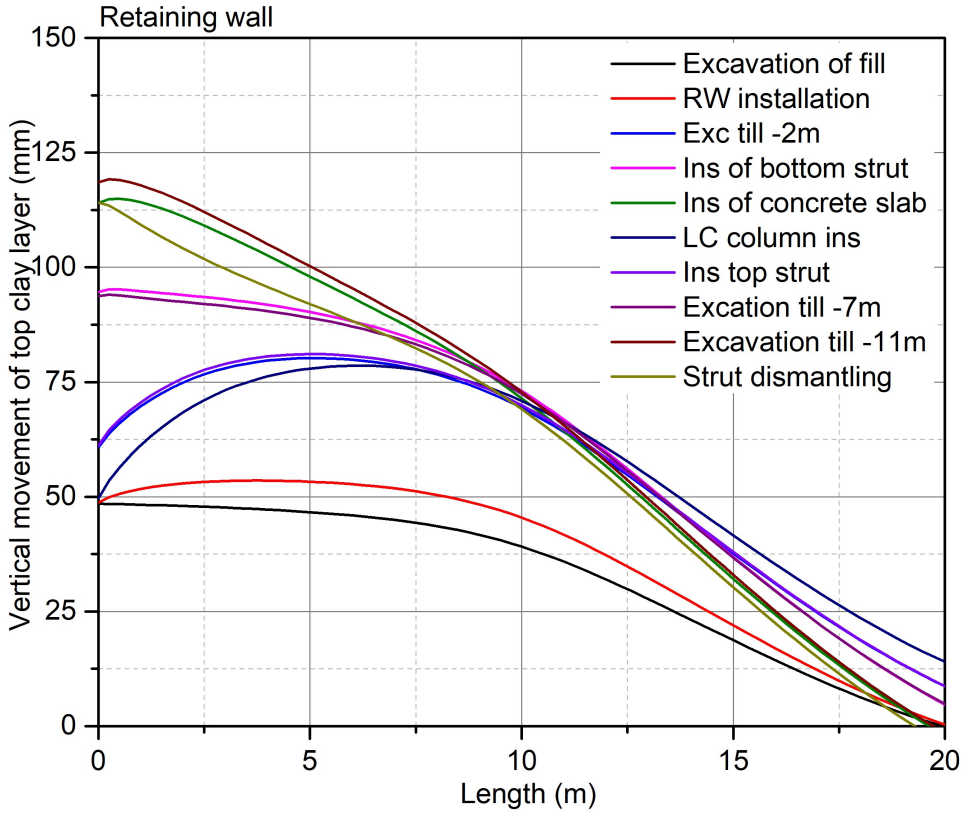

Figure 4.10: Displacement of the top clay layer with adjusted stiffness parameters

4.3 With higher lime-cement stiffness

In figure 4.11 the measured and model prediction using higher lime-cement stiffness is demonstrated. With these set of stiffness values, the predicted and observed wall movements at the initial three stages are matched well. But the displacement at the top of the wall after excavation till level -7 m is predicted outward which is not the case in reality. Other than that, the displacement at the bottom of the wall is estimated sensibly by the model using these sets of lime-cement stiffness.

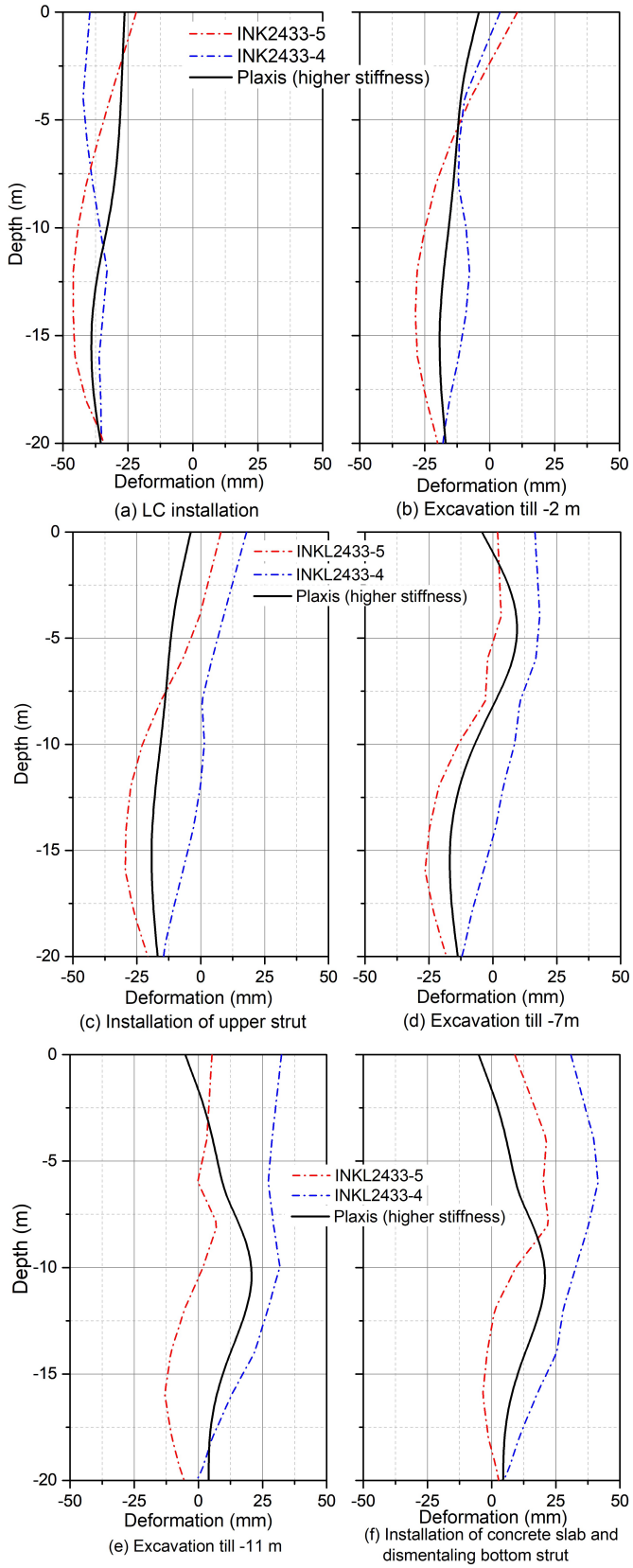

Figure 4.11: Retaining wall movements at various stages of construction [Positive= inward, Negative= outward]

Forces in the top strut are under-predicted by the model (figure 4.12) Initially the force is 1600 kN whereas the field value is around 1800 kN. After excavation till -11 m the calculated forces reduced to 900 kN compared to 1200 kN observed forces. 2100 kN forces are predicted after dismantling the bottom strut which is measured around 2300 kN by the sensors. Forces on the bottom strut are well predicted by the model compared to the field value (1900 kN vs 1700 kN) (Figure 4.13).

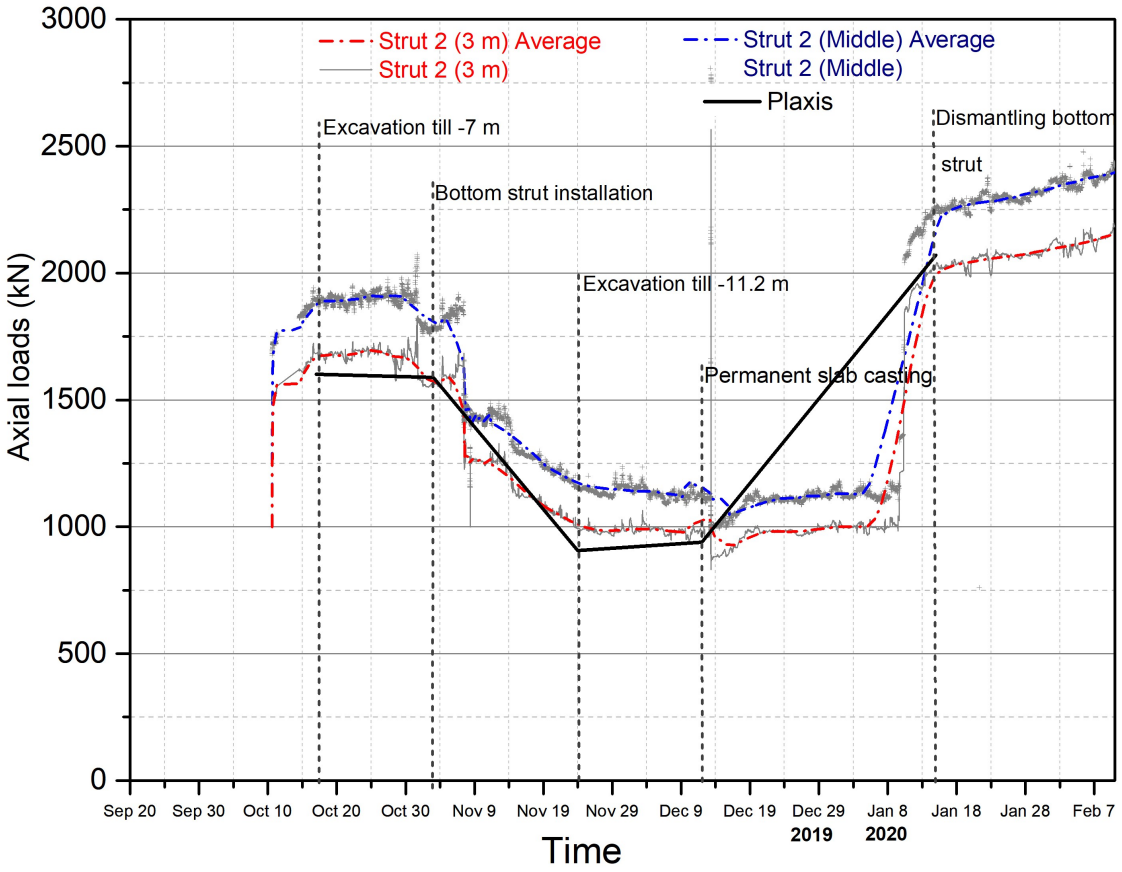

Figure 4.12: Top strut forces with higher stiffness parameters

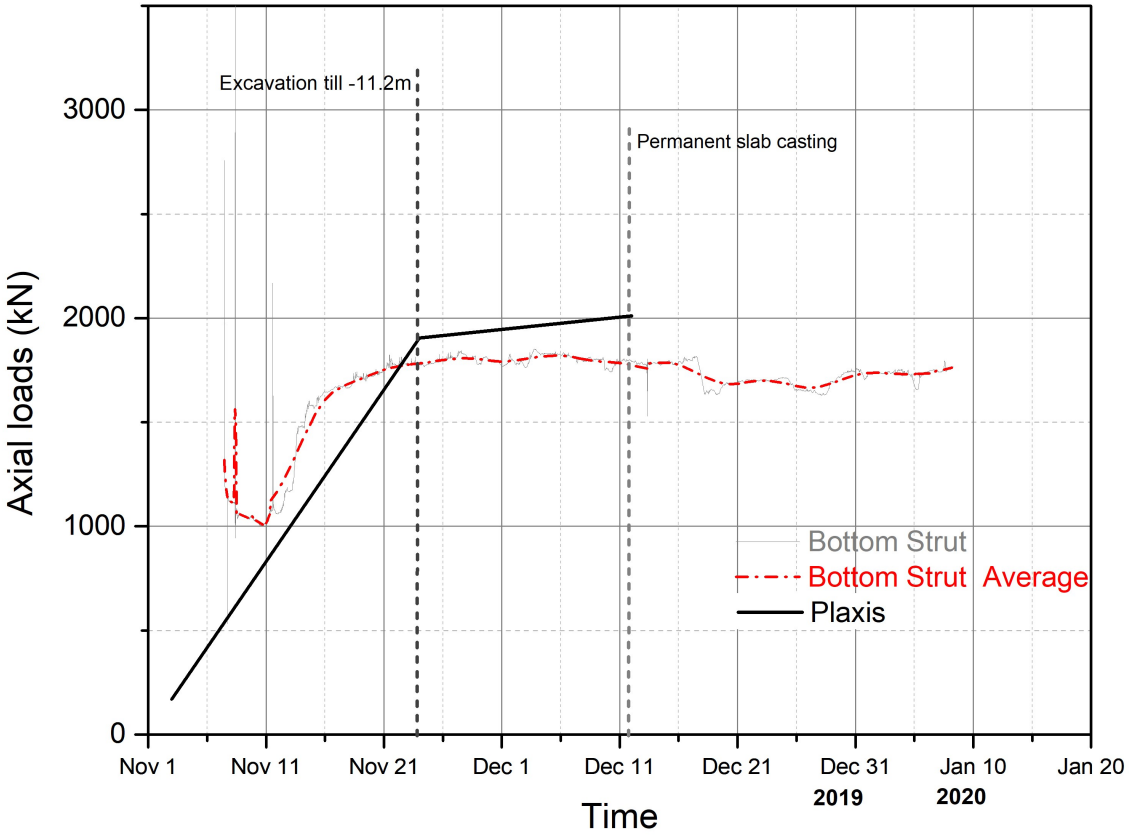

Figure 4.13: Bottom strut forces with higher stiffness parameters

Vertical movements of the excavation bottom at various stages are shown in figure 4.14. The top clay layer movement due to the construction stages is illustrated in figure 4.15. Vertical movement of the clay layer varies between 50 mm and 120 mm at different construction stages which is within the remanded range of Moormann [23].

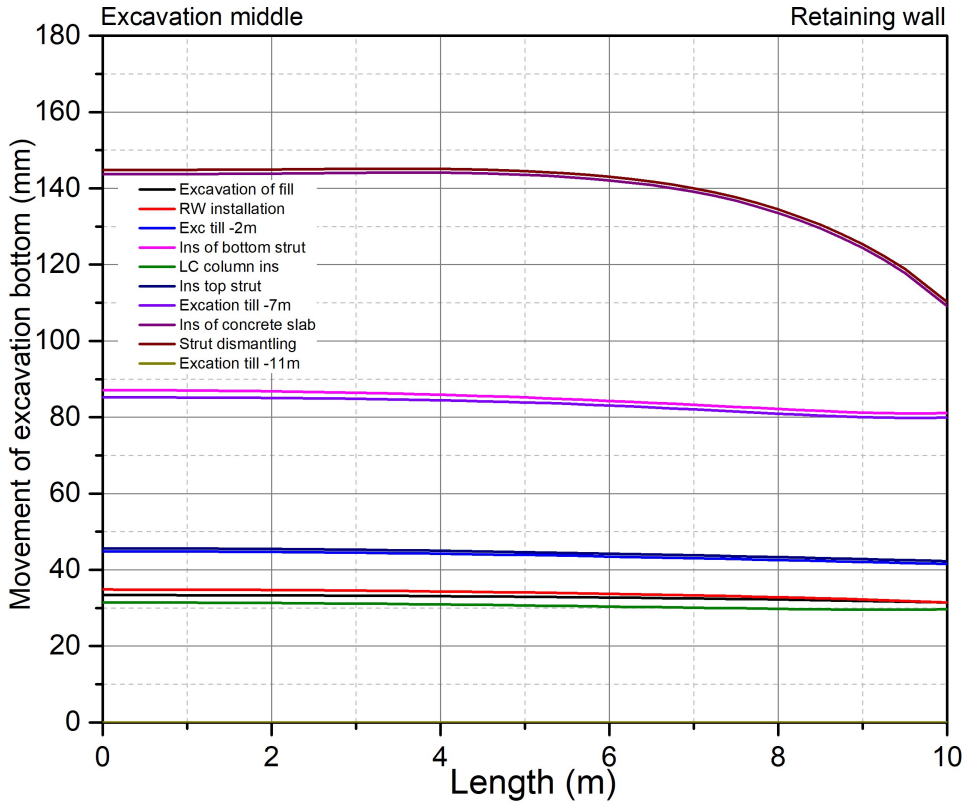

Figure 4.14: Excavation bottom displacement with higher stiffness parameters

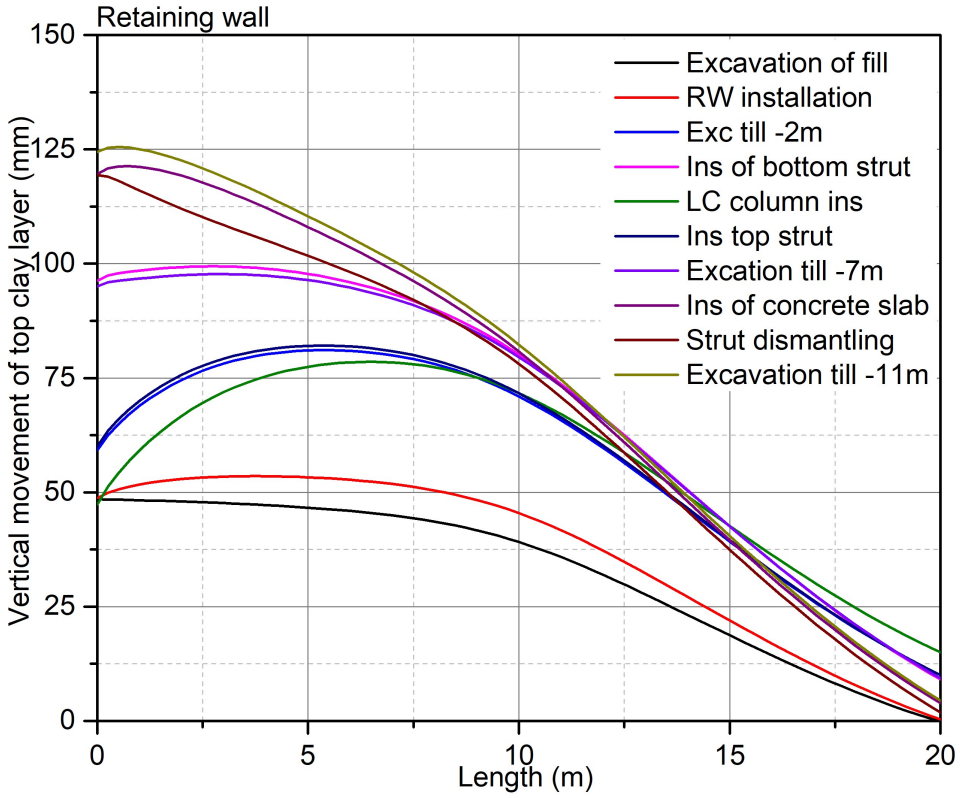

Figure 4.15: Displacement of the top clay layer with higher stiffness parameters

4.4 Comparison

In figure 4.16, the predicted and measured displacements of the retaining wall is illustrated. The red and blue lines are the measured value from inclinometer 2433-5 and 2433-4, black solid line, dash-dot line, and dash line respectively represent plaxis results using adjusted stiffness, initial stiffness, and higher stiffness.
When the lime-cement is inserted in the passive side of the excavation, the predicted wall movement is similar despite changing the stiffness of the composite. After the first excavation till -2 m the initial set of stiffness predicts higher inward movement than the other two sets. But after the excavation till level -11 m the three stiffness set show variations in the displacement prediction. With the initial set of stiffness the wall movement is more towards the excavation, this set over-predicts the wall movement compared to field movement. With the higher stiffness set, the movement at the top of the wall is outward which does not present the field scenario. With the adjusted stiffness set, the wall displacement is reasonable compared to the field observation.

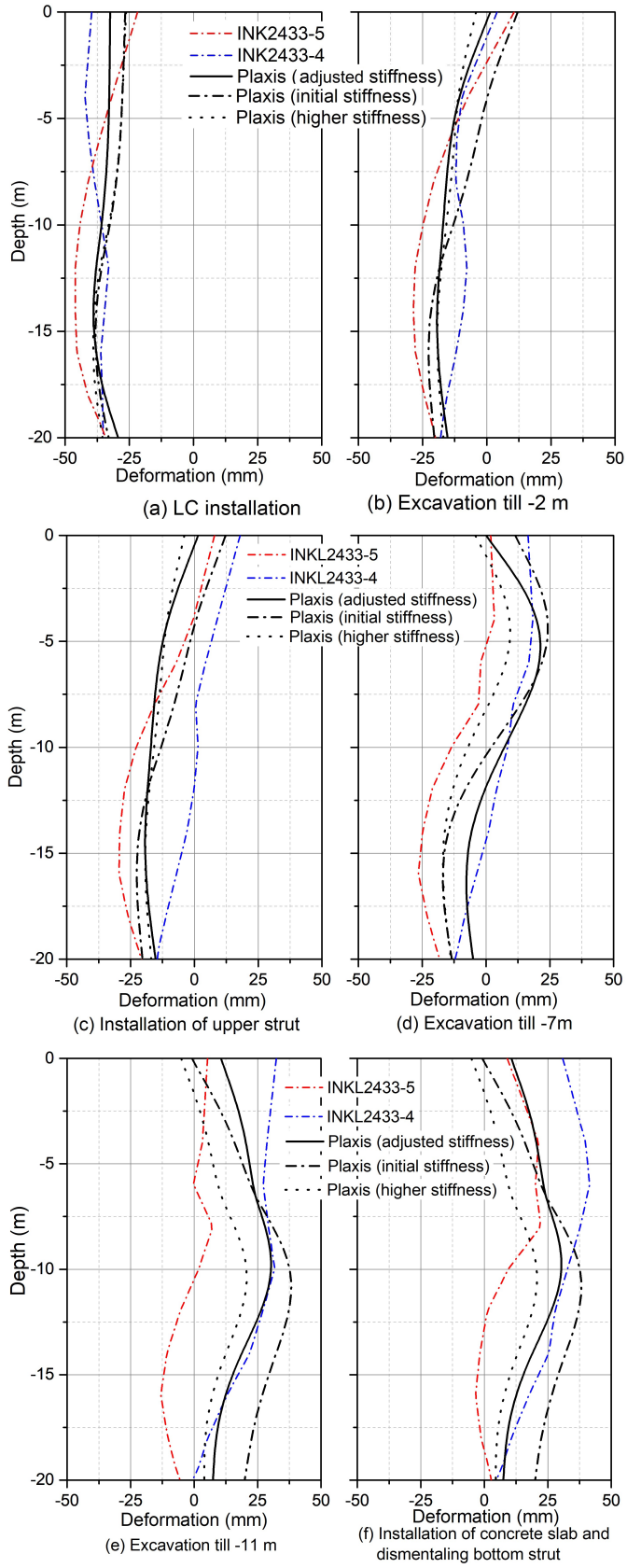

Figure 4.16: Retaining wall movements at various stages of construction [Positive= outward, Negative= inward]

Figure 4.17 and 4.18 represent the forces in the top and bottom struts at different stages with three LC stiffness sets. With higher and initial stiffness set, the top strut forces are under-predicted compared to the observed value. The adjusted stiffness parameters depict the top strut forces in all the stages except the last one where the model over-estimates the force. For bottom strut forces, the higher stiffness set shows a close match compared to field observation. With the adjusted LC stiffness parameters the computed force is 1100 kN higher than the field data.

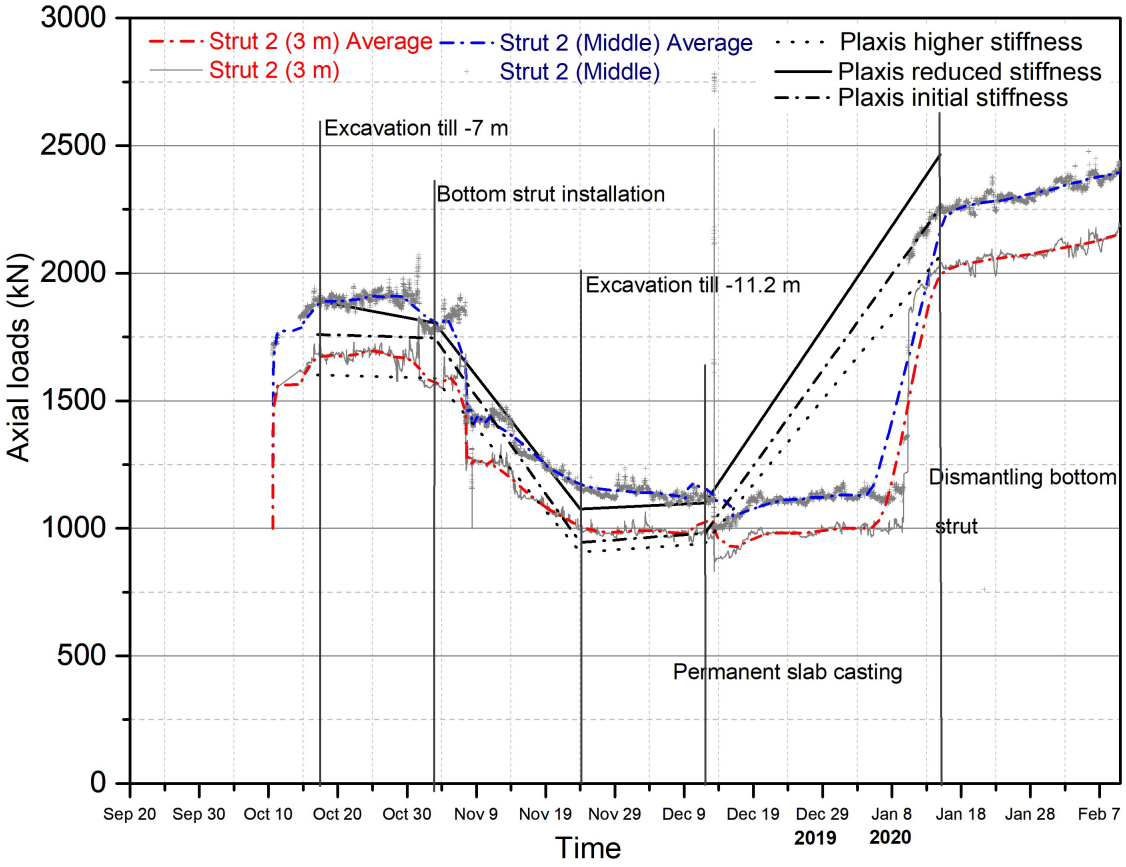

Figure 4.17: Measured and predicted top strut forces

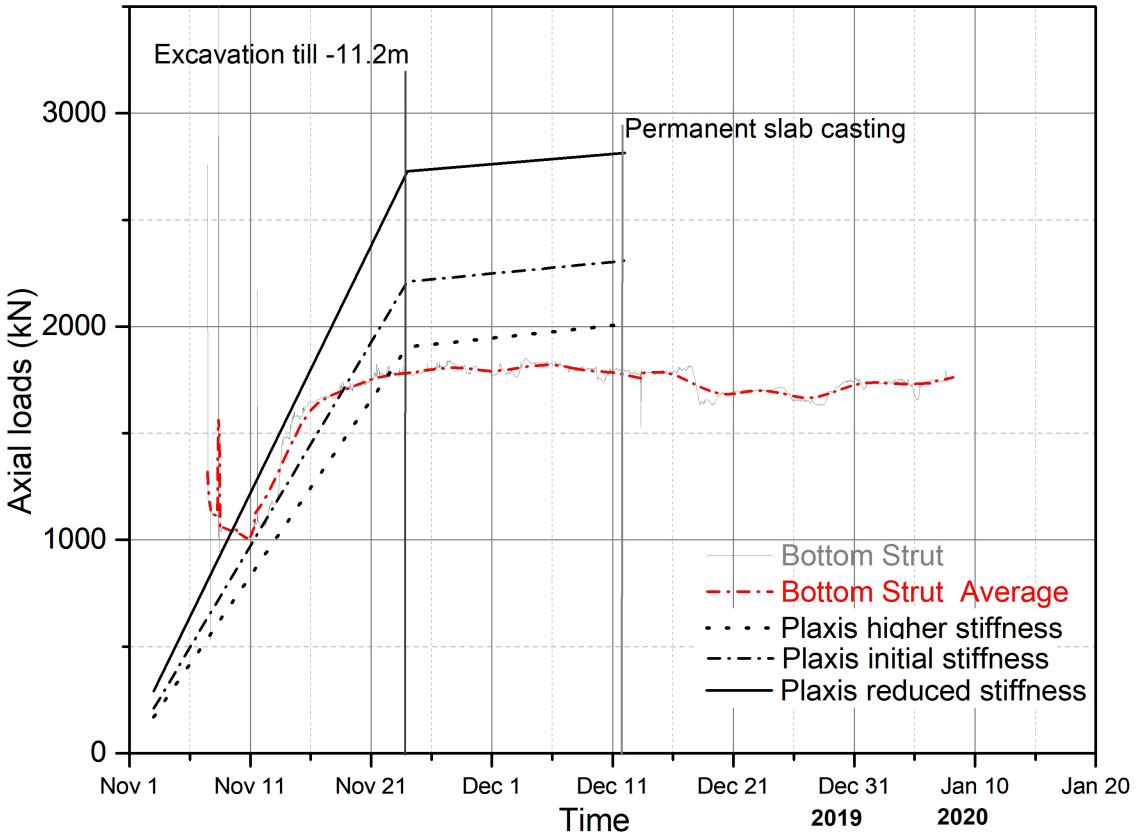

Figure 4.18: Measured and predicted bottom strut forces

The bending moments throughout the retaining wall at three significant stages (Excavation till -7 m, Excavation till -11 m, and Strut dismantling) with three sets of stiffness parameters are shown in figure 4.19. The maximum moment of 550 kN-m/m is found at around 6 m depth during the stage strut dismantling. Lime-cement stiffness variation does not affect much on the bending moments of the wall.

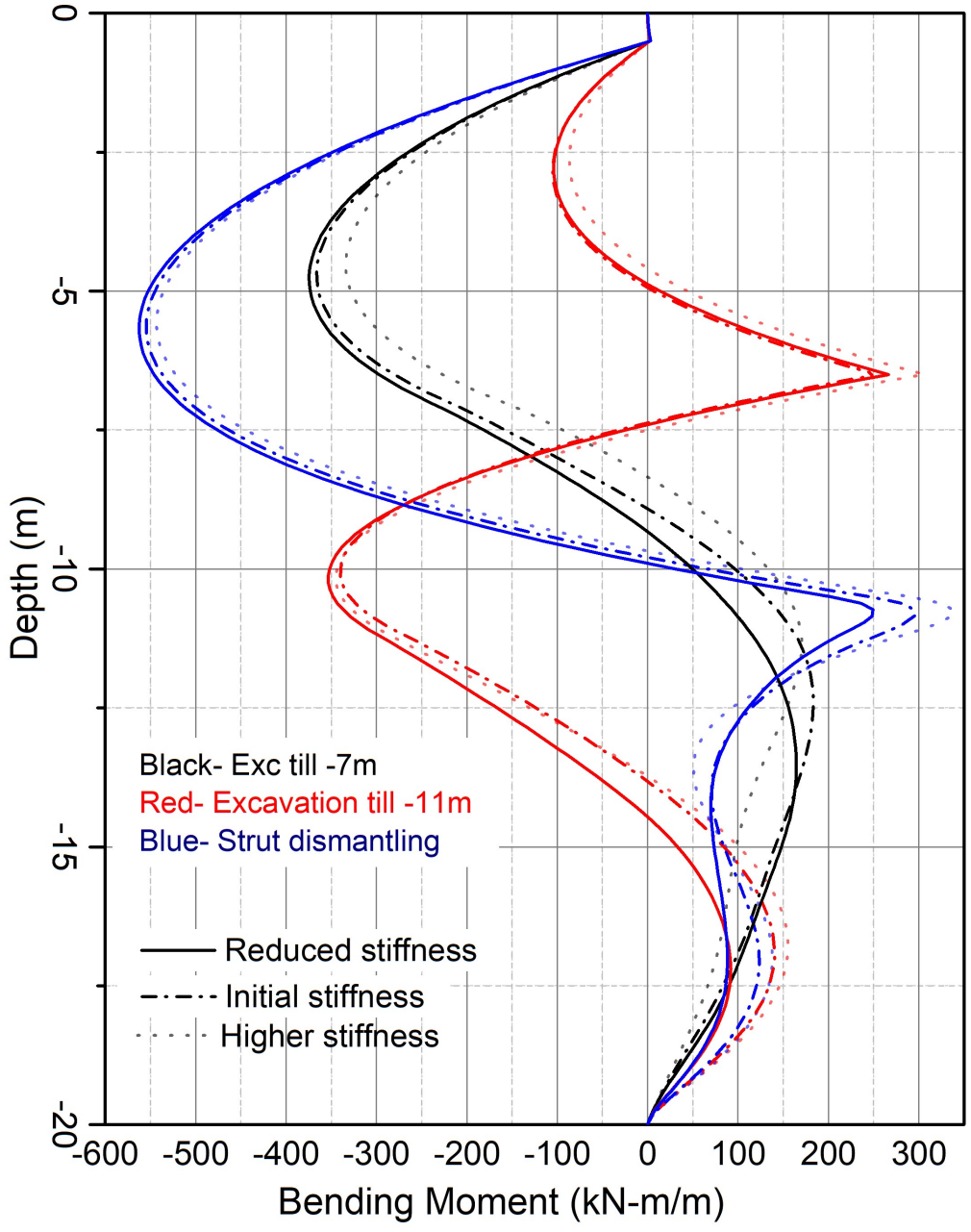

Figure 4.19: Variation of bending moments with different LC stiffness at three individual stages

Variation of shear forces of the wall at three different stages of the construction with three lime-cement stiffness sets is shown in figure 4.20. Change in lime-cement stiffness parameters have a minor effect on the shear forces. The maximum shear force is approximately 380 kN/m at the depth of -11 m during the stage strut dismantling.

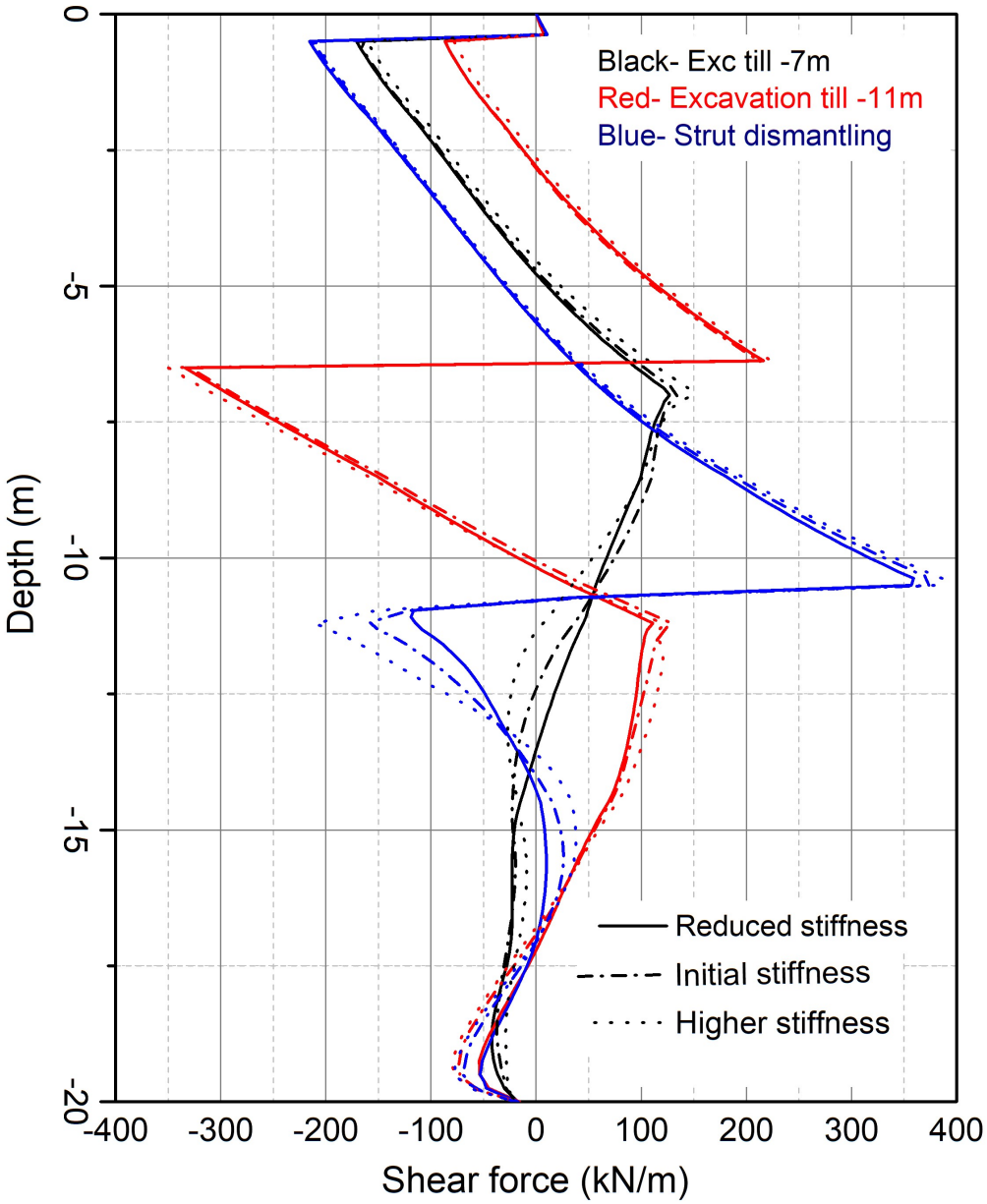

Figure 4.20: Variation of shear forces with different LC stiffness at three individual stages

5
Conclusion

In this thesis, an FE model in plaxis 2D is created to represent the field scenario of a deep excavation in soft soil using lime-cement columns in the passive side. The behavior of the retaining wall at different construction stages is exhibited and compared with the field observed data. From the deformation graphs, it is observed that the model prediction of the displacement matches reasonably with the inclinometer observation. The forces in the top strut are also equitable with the field measurement. But the model fails to calculate the bottom strut forces and over-estimates about 40%.
The lime-cement columns stiffness parameters are adjusted to get reasonable wall deformation and to check the sensitivity of these parameters on the model behavior. The properties of the LC are calculated from lab test and scaled down for the field composite materials using a factor. To approximate this factor, sensitivity analysis of the stiffness parameters are performed. In this specific case, the adjusted set of lime-cement stiffness parameters generate outputs that best-fit the field measurements and the higher stiffness set predicts the strut forces more explicitly than the others. The retaining wall movements are not much sensitive during the early stages but differs after the construction stage excavation till –7 m. The forces on the struts are adequately sensitive to the lime-cement composite stiffness. Also the bending moments and shear forces on the retaining wall follow the same pattern with minor distortion for the three sets of stiffness parameters.
The response of the lime-cement composite is represented by the Hardening Soil model and generates reasonable retaining wall movements and strut forces. This model is reliable to constitute the LC composite behaviors adequately and can be utilized in numerical modelling of the material. In general, numerical models are economical, efficient, and reliable tools to predict soil or composite material behaviors. So numerical models can be used as a design tool for predicting the behavior of excavation in soft soil utilizing LC stabilization in the passive side in the future.

Bibliography

[1] Banerjee, P., and Yousif, N. A plasticity model for the mechanical behaviour of anisotropically consolidated clay. *International Journal for Numerical and Analytical Methods in Geomechanics 10*, 5 (1986), 521–541.

[2] Clough, G. W. Construction induced movements of in situ walls. *Design and performance of earth retaining structures* (1990), 439–470.

[3] Dafalias, Y. Anisotropic critical state clay plasticity model [c]. In *Proceedings of the 2nd International Conference on Constitutive Laws for Engineering Materials* (1987), pp. 513–521.

[4] Das, B. M. Principles of geotechnical engineering/braja m. *Das, Cengage Learning, Stamford, CT* (2011).

[5] Davies, M., and Newson, T. 1993, a critical state constitutive model for anisotropic soils. in predictive soil mechanics. edited by g. t. houlsby and a. n. schofield. thomas telford, london, pp. 219-229.

[6] Ernst, and Sohn. Deutsche gesellschaft für geotechnik. In *Empfehlungen des Arbeitskreis "Baugruben" der Deutschen Gesellschaft für Geotechnik*, vol. 3. Deutsche Gesellschaft für Geotechnik, 1994.

[7] Gens, A., and Nova, R. Conceptual bases for a constitutive model for bonded soils and weak rocks. In *Geotechnical engineering of hard soils-soft rocks* (1993), pp. 485–494.

[8] Ghaboussi, J., and Sidarta, D. New method of material modeling using neural networks. In *Numerical models in geomechanics: NUMOG VI* (1997), pp. 393–400.

[9] Goldberg, D. T., Jaworski, W. E., and Gordon, M. D. Lateral support systems and underpinning. volume 3: Construction methods. Tech. rep., 1976.

[10] Gras, J.-P., Sivasithamparam, N., Karstunen, M., and Dijkstra, J. Permissible range of model parameters for natural fine-grained materials. *Acta Geotechnica 13*, 2 (2018), 387–398.

[11] Hashash, Y. M., and Whittle, A. J. Ground movement prediction for deep excavations in soft clay. *Journal of geotechnical engineering 122*, 6 (1996), 474–486.

[12] Ignat, R., Baker, S., Liedberg, S., and Larsson, S. Behavior of braced excavation supported by panels of deep mixing columns. *Canadian Geotechnical Journal 53*, 10 (2016), 1671–1687.

[13] Irvine, D., and Smith, R. *Trenching practice*. 1992.

[14] Karstunen, M., and Amavasai, A. Best soil: Soft soil modelling and parameter determination, 2017.

[15] Karstunen, M., Krenn, H., Wheeler, S. J., Koskinen, M., and Zentar, R. Effect of anisotropy and destructuration on the behavior of murro test embankment. *International Journal of Geomechanics 5*, 2 (2005), 87–97.

[16] Knappett, J., and Craig, R. F. *Craig's soil mechanics*. CRC press, 2019.

[17] Koskinen, M., Karstunen, M., and Wheeler, S. Modelling destructuration and anisotropy of a natural soft clay. In *NUMGE 2002. 5th European Conference Numerical Methods in Geotechnical Engineering* (2002), pp. 11–19.

[18] Ladd, C. C., and Foott, R. New design procedure for stability of soft clays. *Journal of Geotechnical and Geoenvironmental Engineering 100*, Proc Paper 10064 (1974).

[19] Larsson, S. State of practice report–execution, monitoring and quality control. In *International Conference on Deep Mixing* (2005), pp. 732–785.

[20] Leoni, M., Karstunen, M., and Vermeer, P. Anisotropic creep model for soft soils. *Géotechnique 58*, 3 (2008), 215–226.

[21] Mana, A. I., and Clough, G. W. Prediction of movements for braced cuts in clay. *Journal of Geotechnical and Geoenvironmental Engineering 107*, ASCE 16312 Proceeding (1981).

[22] Massarsch, K., and Topolnicki, M. Regional report: European practice of soil mixing technology. In *Proceeding of International Conference on Deep Mixing–Best Practice and Recent Advances, Stockholm* (2005).

[23] Moormann, C. Analysis of wall and ground movements due to deep excavations in soft soil based on a new worldwide database. *Soils and foundations 44*, 1 (2004), 87–98.

[24] Ou, C.-Y., Wu, T.-S., and Hsieh, H.-S. Analysis of deep excavation with column type of ground improvement in soft clay. *Journal of Geotechnical engineering 122*, 9 (1996), 709–716.

[25] Pakbaz, M., Mehdizadeh, R., Vafaeian, M., and Bagherinia, K. Numerical prediction of subway induced vibrations: case study in iran-ahwaz city. *Journal of applied sciences 9*, 11 (2009), 2001–2015.

[26] Peck, R. B. Deep excavations and tunneling in soft ground. *Proc. 7th ICSMFE, 1969* (1969), 225–290.

[27] Peck, R. B., Hanson, W. E., and Thornburn, T. H. *Foundation engineering*, vol. 10. Wiley New York, 1974.

[28] Porbaha, A. State of the art in deep mixing technology: part i. basic concepts and overview. *Proceedings of the Institution of Civil Engineers-Ground Improvement 2*, 2 (1998), 81–92.

[29] Roscoe, K., and Burland, J. On the generalized stress-strain behaviour of wet clay.

[30] Schanz, T., Vermeer, P., and Bonnier, P. The hardening soil model: formulation and verification. *Beyond 2000 in computational geotechnics* (1999), 281–296.

[31] Sheng, D., Sloan, S., and Yu, H. Aspects of finite element implementation of critical state models. *Computational mechanics 26*, 2 (2000), 185–196.

[32] Sivasithamparam, N., Karstunen, M., and Bonnier, P. Modelling creep behaviour of anisotropic soft soils. *Computers and Geotechnics 69* (2015), 46–57.

[33] STANDARD, B. Execution of special geotechnical works—deep mixing.
[34] Terashi, M. The state of practice in deep mixing methods. In *Grouting and ground treatment*. 2003, pp. 25–49.
[35] Terzaghi, K., Peck, R. B., and Mesri, G. *Soil mechanics in engineering practice*. John Wiley & Sons, 1996.
[36] Trafikverket. The västlänken project in gothenburg, sweden.
[37] Wheeler, S. J., Näätänen, A., Karstunen, M., and Lojander, M. An anisotropic elastoplastic model for soft clays. *Canadian Geotechnical Journal 40*, 2 (2003), 403–418.
[38] Whittle, A. J., and Kavvadas, M. J. Formulation of mit-e3 constitutive model for overconsolidated clays. *Journal of Geotechnical Engineering 120*, 1 (1994), 173–198.
[39] Wood, T. *On the small strain stiffness of some Scandinavian clays and impact on deep excavation*. Chalmers University of Technology, 2016.
[40] Yang, H., Tan, T. S., and Leung, C. F. Mass behaviour of embedded improved soil raft in an excavation. *Proceedings of the Institution of Civil Engineers-Geotechnical Engineering 164*, 1 (2011), 11–25.
[41] Yannie, J., Björkman, T., Isaksson, J., and A, B. Kc-pelare i passivzonnyheten på det geotekniska smörgäsbordet, E02-centralen västlänken. In *GRUNDLÄGGNINGSDAGEN 2020, SGF - Svenska Geotekniska Föreningen* (2020), pp. 57–70.
[42] Yoo, C. Behavior of braced and anchored walls in soils overlying rock. *Journal of geotechnical and geoenvironmental engineering 127*, 3 (2001), 225–233.

A

Appendix A

Table A.1: Initial state of soil layers [39]

Soil layer	Elevation (m)	Unit weight (kN/m^3)	Permeability, $k_x = k_y$ (m/day)	K_0
Fill	2.25 to 0.5	18	7.65	0.5
Clay 1	0.5 to -1.5	16.5	1.0	0.7
Clay 2	-1.5 to -8	15.5	4.0E-5	0.7
Clay 3	-8 to -10	15.7	2.0E-4	0.63
Clay 4	-10 to -14	16.4	4.0E-5	0.61
Clay 5	-14 to -20.5	16.2	4.0E-5	0.61
Clay 6	-20.5 to -30	16.2	3.0E-5	0.58
Clay 7	-30 to -40	16.4	5.0E-5	0.57
Clay 8	-40 to -48	16.5	7.0E-5	0.56
Clay 9	-48 to -100	16.9	2.0E-5	0.57

Table A.2: Properties of sheet pile section AZ38-700N

Structure type	Sectional Area, A (cm^2)	Mass, G (kg/m)	Moment of Inertia, $I_y(cm^4)$	Section Modulus, $W_{el,y}(cm^3)$	Radius of Gyration, $r_g(cm)$
Per Single	161	126.4	66390	2655	20.31
Per Double	322	252.8	132780	5310	20.31
Per meter of wall	230	180.6	94840	3795	20.31

Table A.3: Properties of hollow circular section used as strut

Diameter (mm)	Area, A (cm^2)	Mass, M (kg/m)	Moment of Inertia, $I_y(cm^4)$	Section Modulus, $W_y(cm^3)$	Radius of Gyration, r(cm)
660	288.1	226	150263.04	4553.43	22.84
813	356.35	280	284314.84	6994.21	28.25

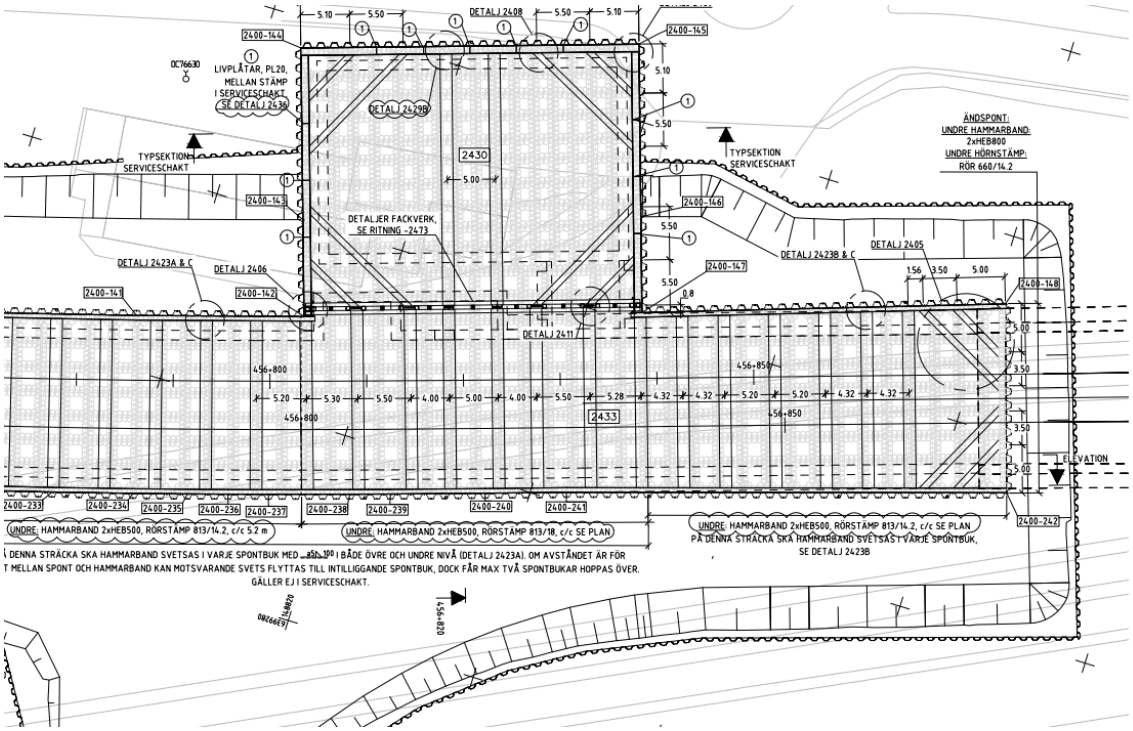

Figure A.1: Orientation of the lower strut level(Datum=-7)

Table A.4: Properties of HEB beam section

Beam Section	Area, A (cm^2)	Mass, M (kg/m)	Moment of Inertia, $I_y(cm^4)$	Section Modulus, $W_y(cm^3)$	Radius of Gyration, r(cm)
HEB 500	238.6	187	12620	842	7.27
HEB 800	334.2	262	14900	993.6	6.68

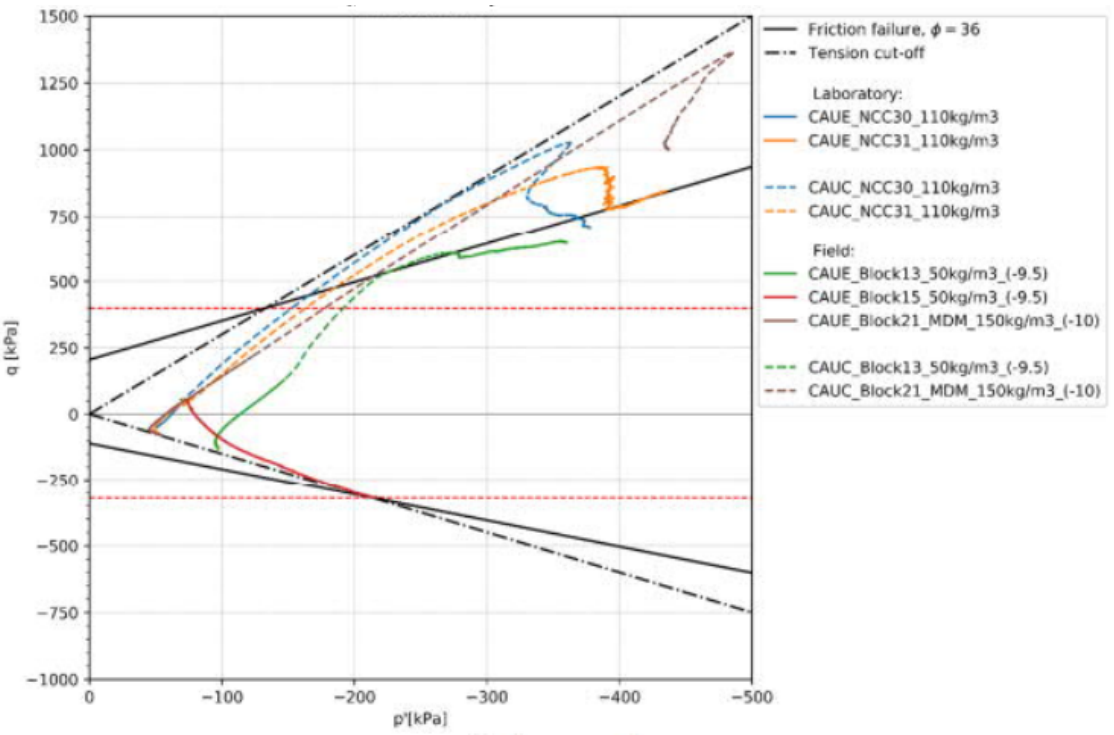

Figure A.2: Lab tests on lime-cement columns (p'-q stress path)

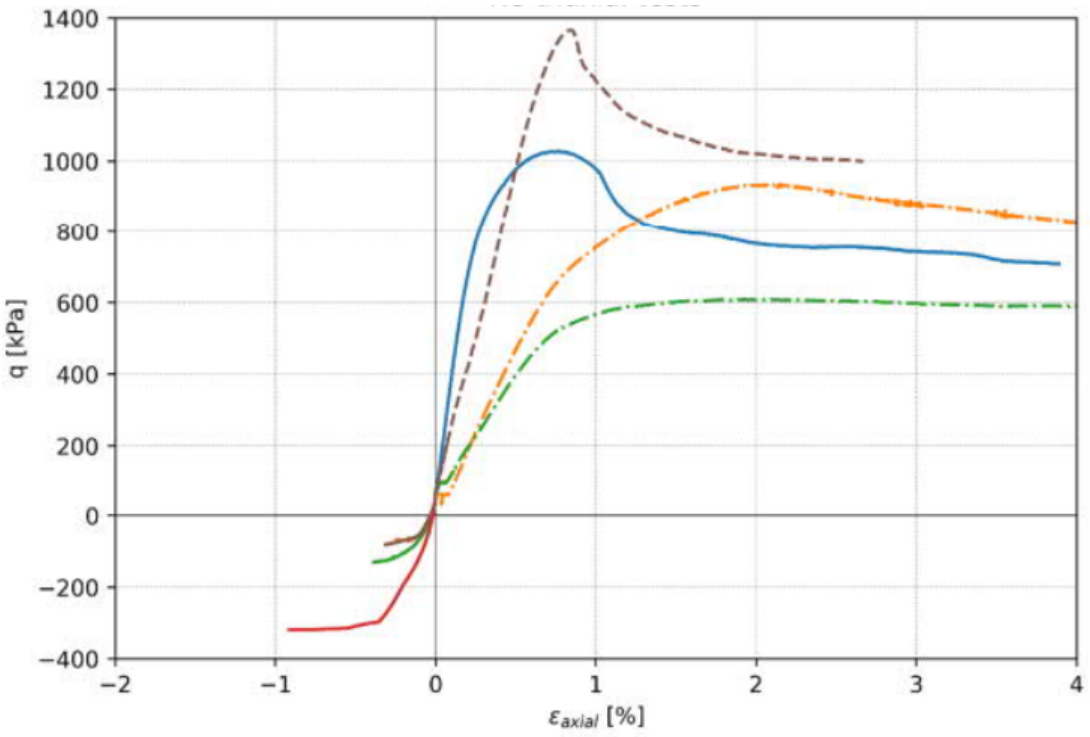

Figure A.3: Lab tests on lime-cement columns (Deviatoric stress vs axial strain)

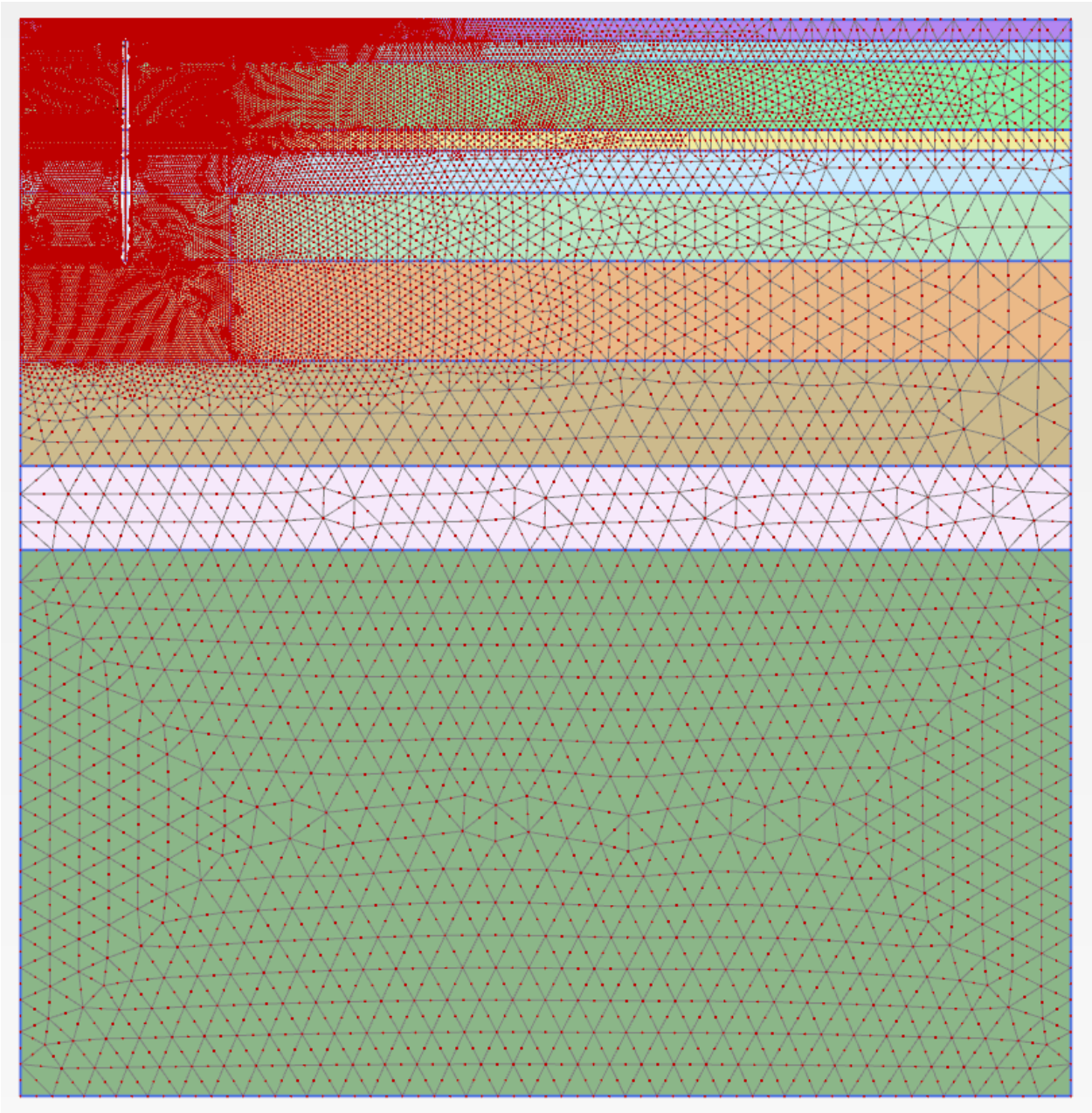

Figure A.4: Mesh geometry of the model

Table A.5: Stiffness from triaxial test on LC samples

Sample	E_{50}^{ref} (MPa)	E_{oed}^{ref} (MPa)	E_{ur}^{ref} (MPa)	ϕ (°)	Type of test
NCC30 (110 kg/m^3)	266.7	133.35	800.10	-	Extension
Block21 (150 kg/m^3, -10 m)	160	80	480	36	Compression
Block13 (50 kg/m^3, -9.5 m)	80	40	240	32	Compression
NCC31 (110 kg/m^3)	85	42.5	255	36	Compression
No.13 (-9.5 m)	50	25	150	37	Compression
No.13 (-9.5 m)	31.82	15.91	95.45	-	Extension
No.15 (-9.5 m)	78.18	39.09	234.55	-	Extension
No.21	181.82	90.91	545.45	36	Compression
No.21	47.27	23.64	141.82	-	Extension
D-14 (-14.01m)	126.67	63.33	380	-	Extension
D-16 (-16m)	175	87.50	525	35	Compression
D-14.2 (-14.2m)	133.57	66.79	400.71	32	Compression
Average	**118.00**	**59.00**	**356**	34.88	-

Table A.6: Parameters of structural elements

Elements	EA	EI ($kN-m^2/m$)	Spacing/ thickness	E (kN/m^2)
Retaining wall	4.6E6 (kN/m)	199.2E3	-	-
Top strut	5.764E6 (kN)	-	10.4	-
Bottom strut	7.127E6 (kN)	-	5.2	-
Concrete slab	-	-	500 mm	33.0E6

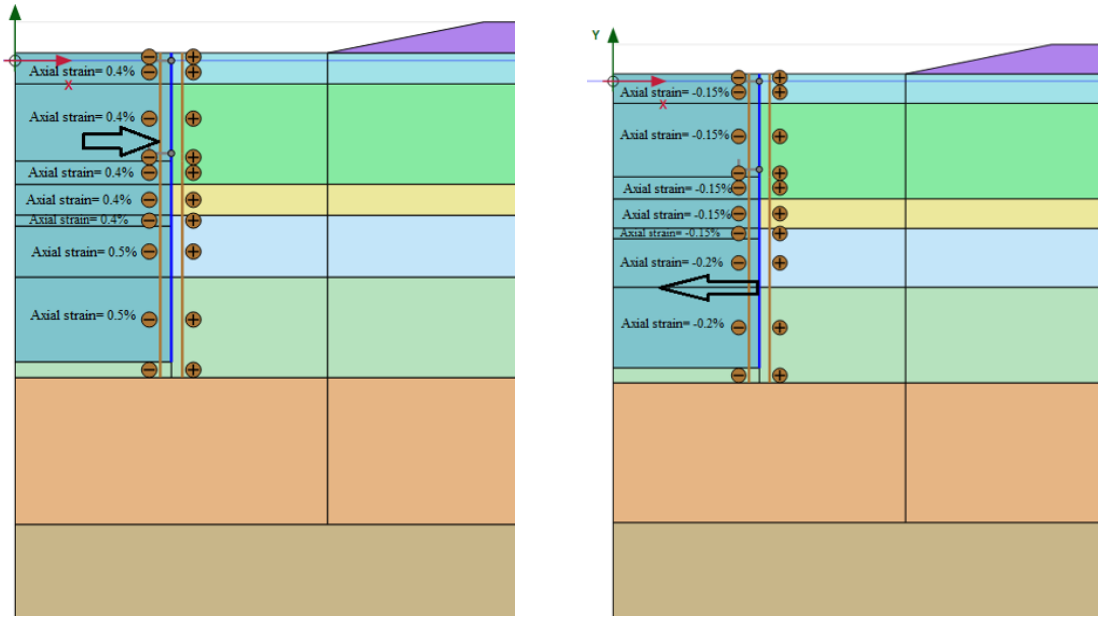

(a) Positive axial strain (outward) **(b)** Negative axial strain (Inward)

Figure A.5: Construction phases